AGU PUBLICATIONS

JGR

Journal of Geophysical Research: Biogeosciences

RESEARCH ARTICLE

10.1002/2016JG003617

Key Points:
- Relationships between concurrent weather conditions and the magnitude of fire activity vary regionally across CONUS
- Concurrent weather conditions affect the magnitude of fire activity via the seasonal duration, spatial extent, and combustion intensity
- Changing weather conditions across CONUS have induced increases in the fire activity season length, burned area, and biomass consumption

Supporting Information:
- Supporting Information S1

Correspondence to:
P. H. Freeborn,
patrickhfreeborn@fs.fed.us

Citation:
Freeborn, P. H., W. M. Jolly, and M. A. Cochrane (2016), Impacts of changing fire weather conditions on reconstructed trends in U.S. wildland fire activity from 1979 to 2014, *J. Geophys. Res. Biogeosci.*, *121*, 2856–2876, doi:10.1002/2016JG003617.

Received 7 SEP 2016
Accepted 25 OCT 2016
Accepted article online 27 OCT 2016
Published online 22 NOV 2016

Impacts of changing fire weather conditions on reconstructed trends in U.S. wildland fire activity from 1979 to 2014

Patrick H. Freeborn[1], W. Matt Jolly[1], and Mark A. Cochrane[2]

[1]US Forest Service, Rocky Mountain Research Station, Fire Sciences Laboratory, Missoula, Montana, USA, [2]Geospatial Sciences Center of Excellence, South Dakota State University, Brookings, South Dakota, USA

Abstract One component of climate-fire interactions is the relationship between weather conditions concurrent with burning (i.e., fire danger) and the magnitude of fire activity. Here daily environmental conditions are associated with daily observations of fire activity within ecoregions across the continental United States (CONUS) by aligning the latter 12 years of a 36 year gridded fire danger climatology with the Moderate Resolution Imaging Spectroradiometer fire products. Results reveal that although modern relationships (2003–2014) vary regionally, fires across the majority of CONUS are more likely to be present and burning more vigorously as fire danger increases. Applying modern relationships to the entire climatology (1979–2014) indicates that in the absence of other influences, changes in fire danger have significantly increased the number of days per year that fires are burning across 42–49% of CONUS (by area) while also significantly increasing daily fire growth and daily heat release across 37–45% of CONUS. Increases in the fire activity season length coupled with an intensification of daily burning characteristics resulted in a CONUS-wide +0.02 $\mathrm{Mha\,yr^{-1}}$ trend in burned area, a 10.6 $\mathrm{g\,m^{-2}\,yr^{-1}}$ trend in the amount of fuel consumed per unit burned area, and ultimately a +0.51 $\mathrm{Tg\,yr^{-1}}$ trend in dry matter consumption. Overall, the results demonstrate regional variations in the response of fires to changes in fire danger and that weather conditions concurrent with burning have a three-pronged impact on the magnitude of fire activity by affecting the seasonal duration, spatial extent, and combustion intensity.

1. Introduction

Climate and land use changes since Euro-American settlement have altered wildland fire regimes across the continental United States, CONUS [*Grissino-Mayer and Swetnam*, 2000; *Heyerdahl et al.*, 2002; *Marlon et al.*, 2012; *Nowacki and Abrams*, 2008]. Deviations from natural and indigenous fire regimes are evidenced by changes over time in attributes such as fire size, intensity, seasonality, and return interval [*Heyerdahl et al.*, 2001; *Miller et al.*, 2009; *Westerling et al.*, 2006]. Shifting fire regimes beyond their historical range and variability redirects successional pathways [*Keane et al.*, 2009; *Keane et al.*, 2004], affects terrestrial carbon sources and sinks [*Hurteau and Brooks*, 2011; *Kashian et al.*, 2006], perturbs the Earth's radiative balance through atmospheric and land cover changes [*Liu et al.*, 2014], and impacts ecosystem services [*Hurteau et al.*, 2014; *Rocca et al.*, 2014]. Such consequences have forced the rethinking of ecologically sustainable fire management [*Keeley et al.*, 2009] and, in light of an expanding wildland fire-urban interface [*Theobald and Romme*, 2007], have forced the reevaluation and reshaping of U.S. wildland fire risk [*Finney*, 2005] and policy [*Stephens and Ruth*, 2005].

The ecological, economic, and health and safety concerns surrounding wildland fires are driving the need to better understand climate-fire relationships. Independent of land use and land management practices, a shift in climatological conditions can influence wildland fire regimes in three ways: first, by altering the environmental gradients that determine the distribution of vegetation fuel types and densities [*Bachelet et al.*, 2001; *Reeves et al.*, 2009]; second, by affecting the atmospheric conditions that promote cloud-to-ground lightning strikes and thus natural ignition sources [*Goldammer and Price*, 1998; *Krause et al.*, 2014; *Price and Rind*, 1994]; and third, by dampening or amplifying the weather and fuel moisture conditions concurrent with majority of burning that influence the probability of new ignitions and subsequent fire behavior [e.g., *Abatzoglou and Kolden*, 2013]. The relative importance of each of these climatic controls on wildland fire activity varies across CONUS [*Littell et al.*, 2009; *Schoennagel et al.*, 2004].

Most if not all recently developed climate-fire relationships include associations between the environmental conditions at the time of burning and the magnitude of wildland fire activity [*Abatzoglou and Kolden*, 2011; *Gedalof et al.*, 2005; *Trouet et al.*, 2009]. Concurrent weather conditions (e.g., solar radiation, air temperature, precipitation, relative humidity, and wind speed) influence the drying and wetting rates of fuel particles, and wildland fires will not spread if fuel moisture contents exceed the moisture of extinction [*Nelson*, 2000]. Thus, weather and fuel moisture conditions regulate the time of year when it is possible for wildland fires to ignite and spread. A greater number of days per year with conducive weather conditions implies more opportunities for wildland fires to be present on the landscape [*Jolly et al*., 2015], and if burning, weather and fuel moisture conditions further affect fire behavior. Lower fuel moisture contents promote faster spread rates, higher reaction intensities, and longer flame residence times [*Anderson*, 1969; *Rothermel*, 1972] as well as less patchy burn patterns [*Slocum et al*., 2003] and greater fuel consumption [*Kauffman and Martin*, 1989; *Knapp et al*., 2005]. Thus, climatic shifts in the weather and fuel moisture conditions immediately preceding ignition and concurrent with burning can alter the seasonal duration, extent, and intensity of wildland fires.

Despite the influences of daily surface weather conditions on multiple, interrelated burning characteristics, most climate-fire relationships only include associations between monthly or seasonally averaged meteorological conditions and total accumulated burned area. To date, the inability to synchronize fire weather with burning characteristics on a daily basis and the use of total burned area as the sole indicator of wildland fire activity largely stems from the fact that fire records such as the Fire Program Analysis-Fire Occurrence Database [*Short*, 2014] and the Monitoring Trends in Burn Severity project [*Eidenshenk et al*., 2007] only contain fire discovery dates and estimates of final fire sizes. In contrast, multispectral imaging systems on board polar orbiting satellites offer repetitive observations of recently burned areas and radiant heat release rates as often as every 3–8 h [*Justice et al*., 2002], enabling daily meteorological conditions (via fire danger indexes) to be aligned with daily fire presence and daily burning characteristics [e.g., *de Groot et al*., 2006; *Dymond et al*., 2005; *Podur and Wotton*, 2011; *Wang et al*., 2014]. Although modern satellite-based fire records offer estimates of several wildland fire attributes unavailable from agency fire reports, the potential of merging daily atmospheric and fuel moisture conditions with coincident satellite observations of wildland fires to elucidate climate-fire relationships remains largely unfulfilled.

The following work reimagines the scope, resolution, and utility of the associations between environmental conditions at the time of burning and the magnitude of wildland fire activity. In section 2 we present a well-known set of equations linking dry matter consumption with burned area, fuel load reduction, and heat release and then reformulate these equations as functions of the location and environmental conditions on the day of burning. In section 3, we describe the use of the U.S. National Fire Danger Rating System (USNFDRS), and specifically the Energy Release Component (ERC), to characterize daily fire weather conditions and also describe the ability of the Moderate Resolution Imaging Spectroradiometer (MODIS) to observe and record daily wildland fire activity across CONUS. In section 4, we use the framework established in section 2 to build empirical relationships between fire danger and fire activity and then use these modern relationships in conjunction with a long-term fire danger climatology to reconstruct regional fire histories across CONUS since 1979. In section 5, we examine geographic variations in the relationships between fire danger and fire activity and examine the isolated impacts of changing fire weather conditions on long-term trends in annual fire activity season length, burned area, fuel consumption, and the amount of fuel consumed per unit area. Finally, in section 6, we discuss the caveats and limitations of this work and highlight the potential of this work to enhance our understanding of climate-fire relationships.

2. Background

The amount of dry matter (DM; kg) consumed during open biomass burning is often estimated using the approach of *Seiler and Crutzen* [1980]:

$$\mathrm{DM} = \mathrm{TBA} \times \mathrm{FL} \times \beta \tag{1}$$

where TBA is total burned area (m^2), FL is the preburn fuel load ($kg\,m^{-2}$), and β is consumption completeness (%). Early inventories typically applied equation (1) over large domains and long time frames using annual burned area, an average fuel loading, and an average consumption completeness [*Leenhouts*, 1998]. Following *Urbanski et al*. [2011], however, dry matter consumption varies spatially across the landscape and seasonally throughout the year so that equation (1) is more appropriately expressed as a function of location, *k*, and time, *t*, as follows:

$$\mathrm{DM}_{k,t} = \mathrm{TBA}_{k,t} \times \mathrm{FLC}_{k,t} \tag{2}$$

where the last two terms on the right-hand side of equation (1) have been consolidated to yield fuel load consumption (FLC; kg m^{-2}). Note that the size, k, and interval, t, can be as small as 500 m grid cells and as short as daily time steps but can be aggregated into larger administrative or ecological units and annual estimates [e.g., *Urbanski et al*., 2011].

Using equation (2) to express dry matter consumption as a function of location and time coincides with the spatiotemporal framework for reporting greenhouse gas emission inventories [*U.S. Environmental Protection Agency*, 2016] and for generating time series maps of source strengths required by smoke injection and transport models [e.g., *Larkin et al*., 2009]. More precisely, however, DM consumption depends on the weather and fuel moisture conditions at the time of burning, represented by the subscript c, and equation (2) can be rewritten accordingly:

$$\mathrm{DM}_{k,c} = \mathrm{TBA}_{k,c} \times \mathrm{FLC}_{k,c} \tag{3}$$

Rather than enumerate all of the environmental conditions encapsulated by c, we hereafter refer to c as fire danger. Fire danger is typically calculated using several surface weather variables (e.g., air temperature, relative humidity, and solar insolation) and may incorporate a fuel model, a fuel moisture model, or a broad-scale topographic classification [*Bradshaw et al*., 1983; *Noble et al*., 1980; *Van Wagner and Pickett*, 1985]. In the context of this work, c represents the fire environment at the time of burning, which includes the current state of the atmosphere as well as the moisture content of large-diameter dead fuels influenced by weather conditions over the previous several weeks before ignition. Since weather and fuel conditions fluctuate daily and seasonally, fire danger, c, is also a function of time. Although the terms in equation (3) can be considered as continuous functions of fire danger, from a computational standpoint, c in this work represents an interval of fire danger.

The first term on the right-hand side of equation (3) represents the distribution of total burned area as a function of fire danger, which can be expanded as follows:

$$\mathrm{TBA}_{k,c} = n_{k,c} \times \mathrm{Pr}_{k,c} \times \overline{\mathrm{DBA}}_{k,c} \tag{4}$$

where $n_{k,c}$ is a number distribution representing the number of days at location k that fall within the fire danger interval, c; $\mathrm{Pr}_{k,c}$ is a location-specific function relating fire danger to the daily probability that a fire is present on the landscape; and $\overline{\mathrm{DBA}}_{k,c}$ (m^2 d^{-1}) is the relationship between fire danger and average daily burned area, calculated using only the days when fires are present on the landscape. In essence, equation (4) is formulated such that the total burned area in a particular location is determined by the following: (i) the climatological distribution of fire danger, (ii) the unconditional probability of fire presence as a function of fire danger, and (iii) the average daily fire growth as a function of fire danger, conditional on the presence of a fire.

If it is assumed that fuel consumption is proportional to the radiant heat released during combustion [*Wooster et al*., 2005], then DM can alternatively be estimated by multiplying the fire radiative energy (FRE) by a radiant consumption factor (RCF), as such,

$$\mathrm{DM}_{k,c} = \mathrm{FRE}_{k,c} \times \mathrm{RCF} \tag{5}$$

where FRE (MJ) is obtained from a time series of radiant heat flux measurements and RCF (kg MJ^{-1}) is determined from laboratory or field measurements [e.g., *Dickinson et al*., 2016; *Freeborn et al*., 2008; *Kremens et al*., 2012]. Although equation (5) is attractive since it circumvents uncertainties in the preburn fuel load and consumption completeness [*Urbanski et al*., 2011], it nevertheless assumes that RCF is independent of fuel type, fuel moisture content, and combustion phase. In reality, RCF at the very least also varies with fuel moisture [*Smith et al*., 2013] and thus fire danger.

Similar to equation (4), the radiant energy emitted from wildland fires burning on days within an interval of fire danger, $\mathrm{FRE}_{k,c}$, can be expressed as follows:

$$\mathrm{FRE}_{k,c} = n_{k,c} \times \mathrm{Pr}_{k,c} \times \overline{\mathrm{DRH}}_{k,c} \tag{6}$$

where $\overline{\mathrm{DRH}}$ is the relationship between fire danger and the mean daily radiant heat release (MJ d^{-1}) averaged over only the days when fires are present on the landscape.

If observations of burned area and FRE are collocated, then equations (2) and (5) can be combined to express fuel load consumption as a function of fire danger:

$$\mathrm{FLC}_{k,c} = \frac{\mathrm{FRE}_{k,c} \times \mathrm{RCF}}{\mathrm{TBA}_{k,c}} \tag{7}$$

It should be warned that in the case of satellite observations, differences in the strategy and performance of different detection algorithms result in estimates of burned area and radiative energy that often do not coincide with the same fire activity. Therefore, pixels recorded in different satellite-based fire products must be spatially and temporally aligned to ensure that burned areas and hot spots are collocated before equation (7) can be used to estimate fuel load consumption [*Andela et al.*, 2016; *Roberts et al.*, 2011].

3. Data Sets

3.1. Daily Fire Danger Grids

Daily environmental conditions at the time of burning are characterized using a fire danger rating index, introduced as the subscript *c* in section 2. Although conceived as an indicator of the fire environment during the first few days of a newly discovered fire [*Deeming et al.*, 1977], fire danger indices are increasingly being used to develop climate-fire relationships through their association with fire growth beyond the origin and start date [*Barbero et al.*, 2014; *Riley et al.*, 2013]. Although several fire danger rating systems are used internationally [e.g., *Noble et al.*, 1980; *Van Wagner and Pickett*, 1985], here we utilize the U.S. National Fire Danger Rating System (USNFDRS) since it is widely applied across CONUS.

The USNFDRS combines standardized fuel models with weather observations to calculate daily indices that reflect a potential fire's physical characteristics during worst-case burning conditions [*Deeming et al.*, 1977]. One USNFDRS output is the Energy Release Component (ERC), which is an index that is related to the available heat per unit area ($\mathrm{kJ\,m^{-2}}$) within the flaming front of a head fire. ERCs are calculated from midafternoon air temperature, relative humidity, and sky cover as well as 24 h maximum and minimum air temperature, relative humidity, and rainfall duration [*Bradshaw et al.*, 1983]. ERC calculations also depend on fuel type and thus the selection of USNFDRS fuel model which varies across CONUS [*Burgan et al.*, 1998]. Fuel model G (typical of dense conifer stands with heavy fuel accumulations) contains a mixture of all dead fuel size classes, as well as a live herbaceous and woody component. Fine dead fuels respond to changes in precipitation and relative humidity quicker than coarse woody debris; therefore, ERCs calculated for NFDRS fuel model G, ERC(G), capture both day-to-day fluctuations and seasonal oscillations in fuel moisture contents. Since the use of a single fuel model permits comparisons between different locations, and since ERC(G) is a common choice for indicating fire danger [*Abatzoglou and Kolden*, 2013; *Finney et al.*, 2011; *Riley et al.*, 2013], we universally use ERC(G) regardless of location or the true fuel characteristics. Hereafter, the parenthetical (G) is dropped for convenience, and it can be assumed that the subscript *c* represents an interval of ERC, where ERC = ERC(G).

Although historically calculated at individual Remote Automated Weather Stations (RAWSs), the advent of spatial climate data sets has enabled the production of daily, high-resolution fire danger grids that often span several decades [*Abatzoglou*, 2013]. Daily, CONUS-wide grids of ERC are generated here from high-resolution surface meteorological variables, which themselves are created by combining two data sets: the North American Land Data Assimilation System Phase 2 [*Mitchell et al.*, 2004] and the Parameter-elevation Regressions on Independent Slopes Model [*Daly et al.*, 2008]. Daily gridded estimates of mean/maximum/minimum temperature, mean/maximum/minimum relative humidity, and rainfall at 4 km resolution were input to the operational algorithms used by the U.S. National Fire Danger Rating System [*Bradshaw et al.*, 1983] to calculate ERCs across the continental United States from 1979 to 2014.

3.2. MODIS Active Fire and Burned Area Products

The MODIS instruments on board NASA's Terra and Aqua satellites together collect between four and six images per day of ground locations across CONUS [*Kaufman et al.*, 1998]. The visible, near-infrared, and shortwave infrared channels are sensitive to changes in surface spectral reflectance caused by the passage of a fire front [*Giglio et al.*, 2009], and the midwave and longwave infrared channels are sensitive to the thermal radiation emitted during combustion [*Wooster et al.*, 2013]. The MODIS direct broadcast (DB) burned area mapping algorithm identifies the day of burning at ~500 m resolution by inspecting a time series of vegetation indexes calculated from 1.2 μm and 2.1 μm surface reflectance measurements [*Giglio et al.*, 2009, 2013]. The MODIS active fire (AF) detection algorithm uses 3.9 μm and 11.0 μm brightness temperatures to identify ~1 km pixel containing thermal anomalies [*Giglio et al.*, 2003, 2016] and also provides an estimate of the instantaneous fire radiative power (FRP) emitted from subpixel flaming and smoldering combustion components [*Kaufman et al*., 1998; *Wooster et al*., 2003]. Daily fire activity across CONUS is characterized here using 12 years (2003–2014) of the MODIS Collection 5.1 burned area (MCD64A1) and Collection 5.1 active fire (MCD14ML) products.

3.3. WWF Terrestrial Ecoregions

All data are spatially sorted using the World Wildlife Fund (WWF) Terrestrial Ecoregions of the World [*Olson et al*., 2001]. The intent of using ecoregions is to organize the fire danger grids and the MODIS fire records into regions with similar climate, vegetation, and, to some degree, land use practices. The continental U.S. is composed of nine biomes, denoting similar bioclimatic zones, within which are nested 72 ecoregions, denoting similar ecosystems. The most homogeneous biome (Flooded Grasslands and Savannas) contains only one ecoregion (Everglades), while the most heterogeneous biome (Temperate Coniferous Forests) contains 23 ecoregions. Ecoregions range in size from 2.0 Mha (Everglades) to 50.7 Mha (Northern Short Grasslands), though not all are contiguous.

4. Methods

Figure 1 illustrates the flow of the methods. Daily fire danger maps (2003–2014) for each ecoregion are intersected with the daily MODIS fire observations (2003–2014). These 12 years of data are used to build modern empirical functions relating fire danger with fire activity, which are then applied to the entire daily fire danger climatology (1979–2014) to reconstruct 36 years of annual fire activity in each ecoregion.

4.1. Fire Danger and Fire Activity Intersections

Daily fire danger maps for each ecoregion are produced by masking the 4 km gridded fire danger domain with the WWF polygons. Fire danger maps for each ecoregion, *k*, are summarized every day, *t*, using the mean ERC $\left(\overline{\mathrm{ERC}}\right)$ calculated over all 4 km grid cells within its boundaries. This generates an ecoregion-level, daily time series of mean fire danger $\left(\overline{\mathrm{ERC}}_{k,t}\right)$ which is normalized to a relative scale using the formula presented by *Viegas et al*. [1999] and reproduced here:

$$\overline{\mathrm{ERC}}'_{k,t} = 100 \times \frac{\overline{\mathrm{ERC}}_{k,t} - \overline{\mathrm{ERC}}_{k,\min}}{\overline{\mathrm{ERC}}_{k,\max} - \overline{\mathrm{ERC}}_{k,\min}} \tag{8}$$

where the subscripts min and max refer to the historical minimum and maximum of the daily ecoregion mean ERCs and the superscript prime indicates a normalized value. In effect, equation (8) ensures that each ecoregion has a common fire danger index scale so that $\overline{\mathrm{ERC}}'_{k,t} = 0$ represents the coolest and wettest conditions and $\overline{\mathrm{ERC}}'_{k,t} = 100$ represents hottest and driest conditions. An example of $\overline{\mathrm{ERC}}'_{k,t}$ is presented for the North Central Rockies Forests (NCRFs) ecoregion in Figure 2.

Daily indicators of ecoregion-wide fire activity are derived from both the MODIS burned area (MCD64A1) and active fire (MCD14ML) products. Burned area pixels are spatially sorted using the transformed image coordinates obtained from 13 MODIS Level 3 tiles covering CONUS [*Wolfe et al*., 1998] and are temporally sorted using the burn date recorded in the MCD64A1 product files. For each day between 2003 and 2014, the number of grid cells with a matching burn date are multiplied by the size of an individual grid cell (~463 m) to generate a daily time series of ecoregion-wide burned area ($\mathrm{DBA}_{k,t}$). An example of $\mathrm{DBA}_{k,t}$ is presented for the North Central Rockies Forests (NCRFs) ecoregion in Figure 2.

MODIS active fire pixels are spatially and temporally sorted using the geographic coordinates and detection times recorded in the MCD14ML product files. The fire radiative energy (FRE, MJ) emitted from all fires burning in an ecoregion over 24 h is estimated from the instantaneous fire radiative power (FRP) measured four times daily. Of the several techniques developed to estimate FRE from sparse observations of FRP [e.g., *Ellicott et al*., 2009; *Kaiser et al*., 2012; *Kumar et al*., 2011], we use a fire-weighted average value of $\omega = 1.686 \times 10^4\,\mathrm{MJ\,MW^{-1}}$ to convert the sum of FRP to FRE [*Freeborn et al*., 2011]. Daily time series of FRE within an ecoregion are generically referred to as the daily radiant heat release, $\mathrm{DRH}_{k,t}$ (Figure 2), which is converted to dry matter consumption using a radiant conversion factor of $\mathrm{RCF} = 0.368\,\mathrm{kg\,MJ^{-1}}$ [*Wooster et al*., 2005].

Independently synchronizing the time series of daily fire danger $\left(\overline{\mathrm{ERC}}'_{k,t}\right)$ with daily burned area ($\mathrm{DBA}_{k,t}$) and daily radiant heat release ($\mathrm{DRH}_{k,t}$) enables the construction of the empirical functions in equations (4) and (6), respectively, for all 72 ecoregions. Calculating the amount of heat released per unit area ($\mathrm{MJ\,m^{-2}}$) or the amount

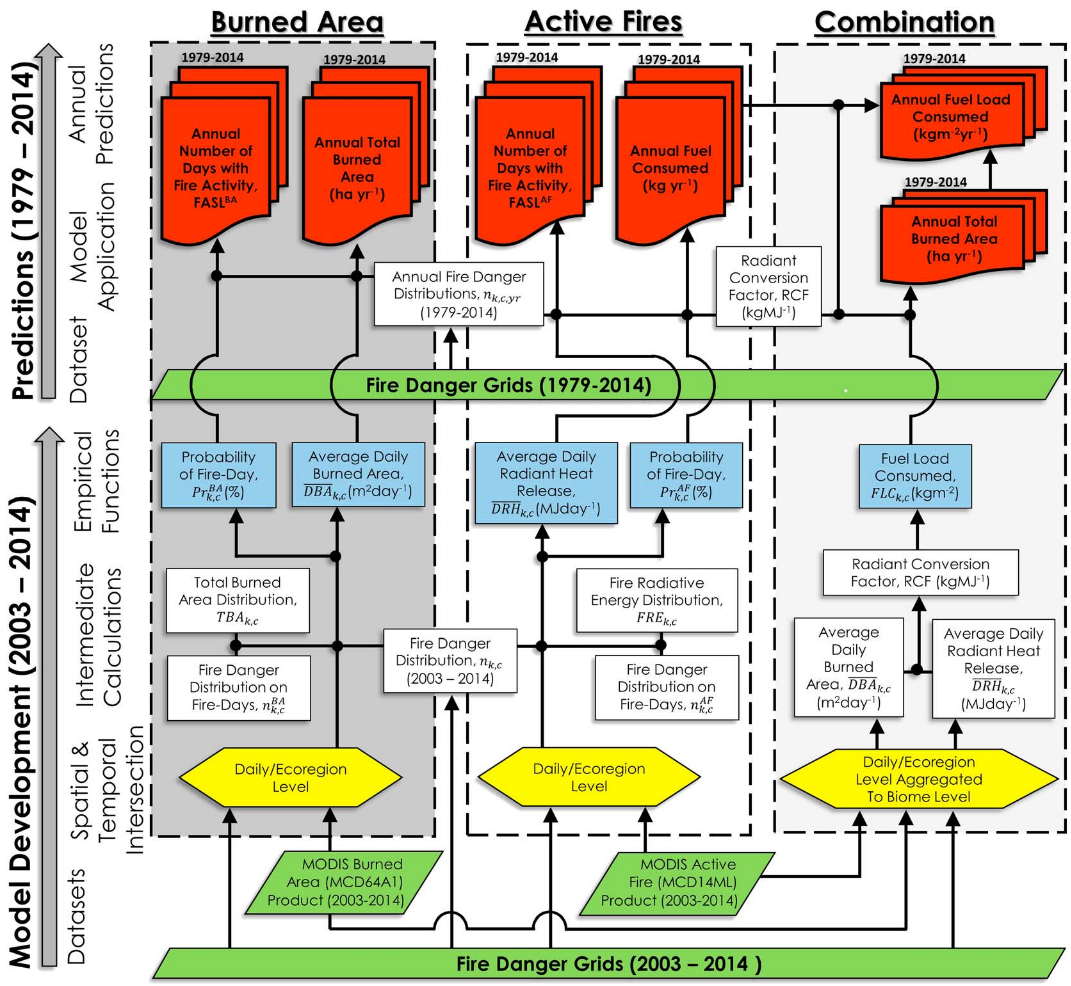

Figure 1. Flow diagram of data sets, model development, and predictions. From the bottom upward, the fire danger grids and satellite observations from 2003 to 2014 are spatially and temporally aligned and used to construct modern empirical functions relating weather conditions with concurrent fire activity. The modern empirical functions are then applied to the entire fire danger climatology to predict annual fire activity from 1979 to 2104. In terms of nomenclature, the subscript *k* represents location, and *c* represents an interval of fire danger.

of fuel consumed per unit area (kg m^{-2}) according to equation (7), however, is complicated by differences in the performance of the different MODIS detection algorithms that results in isolated burned area pixels unaccompanied by active fire pixels, and vice versa. To ensure that the radiant energy detected by MODIS is emitted only from the burned areas also detected by MODIS, we utilize a more refined spatial and temporal intersection procedure whereby (i) burned area pixels are only retained if they fall within the ground footprint of an active fire pixel, (ii) active fire pixels are only retained if their ground footprint contains at least one burned area pixel, and (iii) burned area and active fire pixels are only retained if they are detected within ±8 days of each other. The ground sampling distance between pixel centers as a function of scan angle [*Ichoku and Kaufman*, 2005] is used to roughly define the MODIS active fire pixel ground footprint, while the ±8 day temporal window is applied based on the recommendations of *Roberts et al.* [2011] and *Andela et al.* [2016].

4.2. Empirical Functions

4.2.1. Fire Danger and Fire Activity Distributions

The full range of $\overline{\mathrm{ERC}}'_{k,t}$ is divided into 20 equal-width bins, $c = 1, 2, \ldots, 20$, and all days in the time series are sorted accordingly. The first bin, for example, includes all days when $0 \le \overline{\mathrm{ERC}}'_{k,t} < 5$. The days that fall within

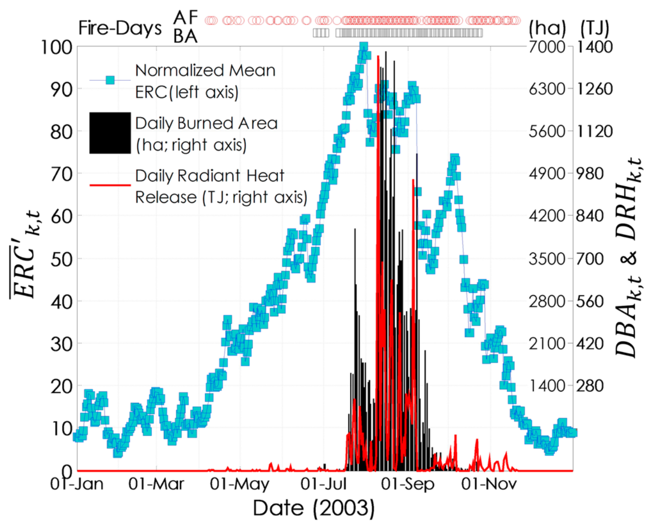

Figure 2. Synchronized daily time series of fire danger and fire activity for the North Central Rockies Forests (NCRFs) ecoregion in 2003. The Energy Release Component (ERC) is averaged over the ecoregion and normalized to its historical maximum. The daily burned area (DBA) and the daily radiant heat release (DRH) are obtained from the MODIS burned area (MCD64A1) and active fire (MCD14ML) products, respectively. Fire days plotted above the axes represent days when MODIS detects at least one burned area (BA) pixel or one active fire (AF) pixel in the ecoregion.

each bin are counted, and the fire danger distribution for each ecoregion ($n_{k,c}$) represents the number of days that occur within an interval of normalized fire danger.

Ecoregion-level fire danger distributions are also constructed using "fire days" only. Similar to a "spread event day" [*Podur and Wotton*, 2011], a fire day is defined here as a day when there is at least one wildland fire burning in an ecoregion that is either large enough or intense enough to trigger the MODIS burned area (BA) or active fire (AF) detection algorithms. An example of the fire days detected by MODIS in the North Central Rockies Forests (NCRFs) is shown in Figure 2. Fire danger distributions on fire days are constructed for each ecoregion by sorting and counting the number of fire days that fall within the same 20 equal-width bins of normalized fire danger, c. Whereas $n_{k,c}$ represents the climatological distribution of fire danger on all days, $n^{BA}_{k,c}$ and $n^{AF}_{k,c}$ represent the distribution of fire danger on only the days when MODIS detects a burned area pixel or an active fire pixel, respectively.

Likewise, distributions of total burned area and fire radiative energy as functions of fire danger ($\mathrm{TBA}_{k,c}$ and $\mathrm{FRE}_{k,c}$) are constructed by summing the burned area and the radiant heat release detected by MODIS on days when $\overline{\mathrm{ERC}}'_{k,t}$ is within the fire danger interval c.

4.2.2. Probability of a Fire Day

In theory, $\mathrm{Pr}_{k,c}$ introduced in equations (4) and (6) represents the likelihood of at least one wildland fire burning in an ecoregion as a function of fire danger. In practice, $\mathrm{Pr}_{k,c}$ expresses the likelihood of MODIS detecting at least one wildland fire in an ecoregion as a function of fire danger and is calculated as the proportion of all days that are fire days (Appendix A). Two sets of probability curves are generated for each ecoregion based on the fire days when MODIS detects a burned area pixel $\left(\mathrm{Pr}^{BA}_{k,c}\right)$ or an active fire pixel $\left(\mathrm{Pr}^{AF}_{k,c}\right)$, respectively. Moreover, there are 13 probability curves generated for both $\mathrm{Pr}^{BA}_{k,c}$ and $\mathrm{Pr}^{AF}_{k,c}$: one curve generated using each of the 12 individual years of data plus one mean curve generated using the aggregate of all 12 years of data. Note that the probability curves derived from the two different MODIS fire products are not interchangeable; rather, $\mathrm{Pr}^{BA}_{k,c}$ and $\mathrm{Pr}^{AF}_{k,c}$ are specific to equations (4) and (6), respectively.

To summarize and compare the empirical probability curves between the 72 ecoregions across CONUS, we calculate the ratio of the probability of a fire day occurring at high fire danger $\left(70 \leq \overline{\mathrm{ERC}}' < 90\right)$ versus low fire danger $\left(10 \leq \overline{\mathrm{ERC}}' < 30\right)$. This ratio is identified as ρ_{Pr} (Appendix A). Although subjective, selecting the low and high fire danger bins used here excludes the few number of days at the very low and very high ends of the fire danger spectrum and also excludes days of moderate fire danger that likely include transitions in weather conditions and fire activity.

4.2.3. Average Daily Burned Area and Heat Release

The last term in equation (4) represents the average burned area per fire day as a function of fire danger ($\overline{\mathrm{DBA}}_{k,c}$; Appendix A) and is calculated by dividing the total burned area distribution ($\mathrm{TBA}_{k,c}$) by the fire danger distribution on fire days only $\left(n_{k,c}^{BA}\right)$. The last term in equation (6) represents the average radiant heat release per fire day as a function of fire danger ($\overline{\mathrm{DRH}}_{k,c}$; Appendix A) and is calculated by dividing the fire radiative energy distribution ($\mathrm{FRE}_{k,c}$) by the fire danger distribution on fire days only $\left(n_{k,c}^{AF}\right)$. Like the probability curves, there are 13 empirical functions relating ecoregion-wide fire danger to average daily burned area and average daily radiant heat release: one function generated using each of the 12 individual years of data plus one mean curve generated using the aggregate of all 12 years of data. And also, like the probability curves, the ratios $\rho_{\overline{\mathrm{DBA}}}$ and $\rho_{\overline{\mathrm{DRH}}}$ (Appendix A) are used to gauge the relative difference in burning characteristics observed by MODIS at high $\left(70 \leq \overline{\mathrm{ERC}}' < 90\right)$ versus low fire danger $\left(10 \leq \overline{\mathrm{ERC}}' < 30\right)$.

4.2.4. Fuel Load Consumption

Excluding spatially and temporally isolated burned area and active fire pixels (section 4.1) reduced the data sets to 75% and 36% of their original numbers. Moreover, the spatiotemporal matching procedure eliminated 43% of burned area pixels and 90% of active fire pixels detected at low fire danger $\left(\overline{\mathrm{ERC}}' < 50\right)$. At this stage in the methods, a lack of coincident burned area and active fire pixels, especially at low fire danger, severely hindered the development of coherent relationships between fire danger and fuel load consumption at the ecoregion level. Instead, coincident observations were aggregated from ecoregions into biomes, and fuel load consumption as a function of fire danger ($\mathrm{FLC}_{k,c}$) was calculated via equation (7), with k in this case representing a biome.

4.3. Annual Predictions

Modern empirical functions (2003–2014) developed in section 4.2 are applied to the entire 36 year fire danger climatology to predict the annual burned area and FRE that MODIS would have observed in each ecoregion:

$$\mathrm{TBA}_{k,\mathrm{yr}} = \sum_{c=1}^{20} n_{k,c,\mathrm{yr}} \times \mathrm{Pr}_{k,c}^{BA} \times \overline{\mathrm{DBA}}_{k,c} \tag{9}$$

$$\mathrm{FRE}_{k,\mathrm{yr}} = \sum_{c=1}^{20} n_{k,c,\mathrm{yr}} \times \mathrm{Pr}_{k,c}^{AF} \times \overline{\mathrm{DRH}}_{k,c} \tag{10}$$

where $n_{k,c,\mathrm{yr}}$ is the annual fire danger distribution for each year, yr = 1979, 1980, …, 2014. Predictions of annual FRE (MJ) are converted into estimates of annual DM (kg) consumption using a conversion factor of 0.368 kg MJ^{-1} [*Wooster et al*., 2005]. To bound the uncertainty in the annual predictions, 13 sets of linked empirical functions (one for each of the 12 individual years of data plus one mean curve for the aggregate of all 12 years of data) are applied to the fire danger climatology to generate 13 estimates of annual burned area and FRE for every ecoregion and for every year from 1979 to 2014.

Annual predictions of burned area and dry matter consumption from equations (9) and (10) can be decomposed into two parts: the annual number of days that wildland fires are burning on the landscape and the average daily burning rate. These two parameters are decoupled by calculating the fire activity season length (FASL). When multiplied and summed, the first two terms on the right-hand side of equations (9) and (10) represent the FASL or the number of days per year that MODIS is expected to detect at least one burned area (BA) pixel or one active fire (AF) pixel, respectively. Two different versions of the fire activity season length ($\mathrm{FASL}_{k,\mathrm{yr}}^{BA}$ and $\mathrm{FASL}_{k,\mathrm{yr}}^{AF}$) are obtained for every ecoregion and every year based on the empirical functions derived separately from the MODIS burned area and active fire products (Appendix A). Calculating the FASL enables trends in annual burned area and dry matter consumption to be attributed to either (i) an increase in the number of days that fires are burning on the landscape or (ii) an intensification of average daily burning characteristics.

It is extremely important to remember that the empirical functions used in equations (9) and (10) are derived independently from the MODIS burned area and active fire products, respectively. Therefore, the time series of annual TBA and FRE obtained from equations (9) and (10) represent two different reconstructed fire histories and cannot be merged to estimate the radiant heat release per unit area or the amount of fuel consumed per unit area. The use of equation (9) is referred to as the "direct" method for predicting annual burned area since it relies on modern associations developed directly from the MODIS burned area product.

Annual burned area is also estimated here using an "indirect" method that invokes equation (7) to convert daily radiant heat release into daily burned area:

$$\mathrm{TBA}_{k,\mathrm{yr}} = \sum_{c=1}^{20} n_{k,c,\mathrm{yr}} \times \mathrm{Pr}^{\mathrm{AF}}_{k,c} \times \overline{\mathrm{DRH}}_{k,c} \times \mathrm{RCF} \times \mathrm{FLC}^{-1}_{k,c} \tag{11}$$

The use of equation (11) circumvents differences between the MODIS burned area and active fire products and uses the empirical relationship between fuel load consumption and fire danger to estimate the burned area that contributed to the MODIS measurements of FRE. Ultimately, equations (10) and (11) are used to predict annual fuel load consumption ($\mathrm{FLC}_{k,\mathrm{yr}}$) for every biome and every year from 1979 to 2014.

5. Results

Results are divided into two sections: a description of the empirical functions developed by associating daily fire danger with daily observations of fire activity from 2003 to 2014 (section 5.1) and a summary of the predictions of annual fire activity from 1979 to 2014 (section 5.2). Results in these two sections are further organized in order of increasingly coarser spatial resolutions, from an individual ecoregion to CONUS.

5.1. Empirical Functions

An example of the empirical functions relating fire danger with MODIS observations of fire activity is presented in section 5.1.1 for a single ecoregion: the North Central Rockies Forests (NCRFs). Rather than presenting every empirical function for all 72 ecoregions across CONUS, ecoregion-level relationships between fire danger and fire activity are summarized and compared in section 5.1.2 based on the ratios (ρ) used to gauge the relative difference in burning characteristics observed by MODIS at high versus low fire danger. For transparency, however, examples of empirical functions for 11 ecoregions within eight biomes are presented in the supporting information (Figures S1–S12).

5.1.1. The North Central Rockies Forests

The fire danger distribution of all days ($n_{k,c}$) in the NCRF from 2003 to 2014 is right skewed, indicating a greater number of days with low to moderate fire danger conditions (Figures 3a and 4a). In contrast, fire danger distributions on fire days when MODIS detected a burned area pixel or an active fire pixel ($n^{\mathrm{BA}}_{k,c}$ and $n^{\mathrm{AF}}_{k,c}$) are left skewed (Figures 3a and 4a), indicating that during the 12 years study period MODIS more often detected evidence of wildland fires in the NCRF on hotter and drier days. Likewise, distributions of total burned area and FRE as functions of fire danger ($\mathrm{TBA}_{k,c}$ and $\mathrm{FRE}_{k,c}$) are left skewed (Figures 3b and 4b). From 2003 to 2014, MODIS detected 89% of the burned area and 79% of the FRE in the NCRF when fire danger exceeded 70% of its historical maximum $\left(\overline{\mathrm{ERC}}' \geq 70\right)$, reflecting the high concentration of fire activity (mainly uncontrolled wildland fires) burning during hot and dry weather conditions.

The probability of MODIS detecting a burned area pixel or an active fire pixel ($\mathrm{Pr}^{\mathrm{BA}}_{k,c}$ and $\mathrm{Pr}^{\mathrm{AF}}_{k,c}$) is low at low fire danger and increases as fire danger increases until it is almost guaranteed that MODIS will detect at least one wildland fire in the NCRF on days of extreme fire danger (Figures 3c and 4c). On average in the NCRF, MODIS is 40.2 times $\left(\rho^{\mathrm{BA}}_{\mathrm{Pr}}\right)$ and 5.4 times $\left(\rho^{\mathrm{AF}}_{\mathrm{Pr}}\right)$ more likely to detect a burned area pixel and an active fire pixel, respectively, on days during high fire danger $\left(70 \leq \overline{\mathrm{ERC}}' < 90\right)$ versus low fire danger $\left(10 \leq \overline{\mathrm{ERC}}' < 30\right)$. The value of the probability ratios (which reflects the shape of the probability curves) for the NCRF is indicative of a fire regime where the fire activity and fire weather seasons are synchronized, and the peak in fire occurrence (mainly uncontrolled wildfires) coincides with the peak in hot, dry weather conditions (Figure 2). The NCRF did not experience the same fire danger every year, nor did it burn in the same manner every year. Consequently, interannual fluctuations in fire weather and fire activity in the NCRF induced variability in the set of empirical probability curves derived for each of the 12 years in the study period (Figures 3c and 4c).

The average daily burned area $\left(\overline{\mathrm{DBA}}_{k,c}\right)$ and the average daily radiant heat release $\left(\overline{\mathrm{DRH}}_{k,c}\right)$ detected by MODIS both increased exponentially by 2 orders of magnitude over the full spectrum of fire danger in the NCRF (Figures 3d and 4d). Based on the accumulation of all 12 years of data, MODIS estimates of daily fire growth and radiant heat release are 17.7 times $\left(\rho_{\overline{\mathrm{DBA}}}\right)$ and 8.8 times $\left(\rho_{\overline{\mathrm{DRH}}}\right)$ greater at high fire danger compared to low fire danger, reflecting an intensification of daily burning characteristics during hot and dry

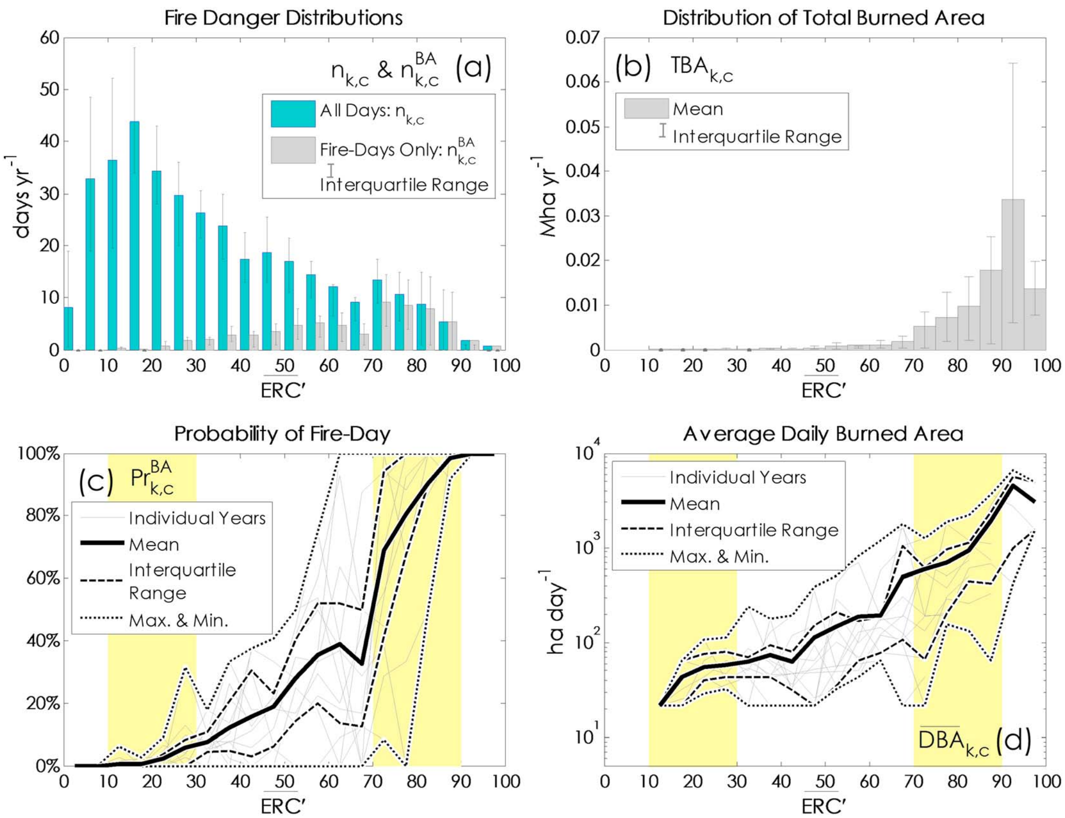

Figure 3. Graphical depiction of equation (4) for the North Central Rockies Forests (NCRFs) ecoregion, identified by the subscript k. (a) The fire danger distribution as a function of the Energy Release Component (ERC) for all days, $n_{k,c}$, alongside the fire danger distribution on fire days only when MODIS detects at least one burned area (BA) pixel. (b) The distribution of total burned area detected by MODIS as a function of ERC. (c) The probability curve $Pr^{BA}_{k,c}$ indicates the likelihood of MODIS detecting at least one BA pixel in the ecoregion as function of ERC. (d) The average burned area per fire day, $\overline{DBA}_{k,c}$. Note the log scale in Figure 3d. The yellow bands centered at $\overline{ERC}' = 20$ and $\overline{ERC}' = 80$ illustrate the low and high fire danger intervals over which the ratios, ρ, are calculated (see Figure 5).

weather conditions. Like the probability curves, relationships between fire danger and fire activity in the NCRF varied from year to year, with interannual values of $\rho_{\overline{DBA}}$ ranging from 0.5 to 29.7 and $\rho_{\overline{DRH}}$ ranging from 0.4 to 15.0 (Figures 3d and 4d).

5.1.2. Ecoregion-Level Summaries

The shapes and magnitudes of the ecoregion-level probability curves varied across CONUS, as illustrated by geographical differences in the probability ratios (Figures 5a and 5b), suggesting regional difference in the presence of wildland fires under similar weather conditions. Technically, ecoregions with $\rho_{Pr}=1.0$ indicate that there is an equivalent chance of MODIS detecting wildland fires on days with high and low fire danger, while values of $\rho_{Pr}>1.0$ indicate that MODIS is more likely to detect a wildland fire on days with higher fire danger. However, in terms of characterizing wildland fire regimes, ecoregions with $\rho_{Pr}=1.0$ indicate that wildland fires are equally likely to be burning regardless of weather conditions, and ecoregions with $\rho_{Pr}>1.0$ indicate that wildland fires are more likely to be burning during hotter and drier conditions. In general, MODIS is more likely to detect a wildland fire on days with high fire danger compared to low fire danger, with probability ratios derived from the burned area and active fire products (ρ^{BA}_{Pr} and ρ^{AF}_{Pr}) exceeding 1.0 in ecoregions accounting for 98% of CONUS by area. Moreover, probability ratios exceeded 5.0 in ecoregions accounting for 44–57% of CONUS by area, indicating locations where the peak in fire occurrence is strongly synchronized with the peak in the fire weather season.

Although Figures 5a and 5b suggest that wildland fires across the majority of CONUS are less likely to be burning at low fire danger, it is also quite possible that the MODIS detection performance degrades on days with lower ERCs due to the smaller and/or lower intensity fires burning during cooler, moister conditions or the increased cloud cover that typically accompanies lower fire danger and obscures the land surface.

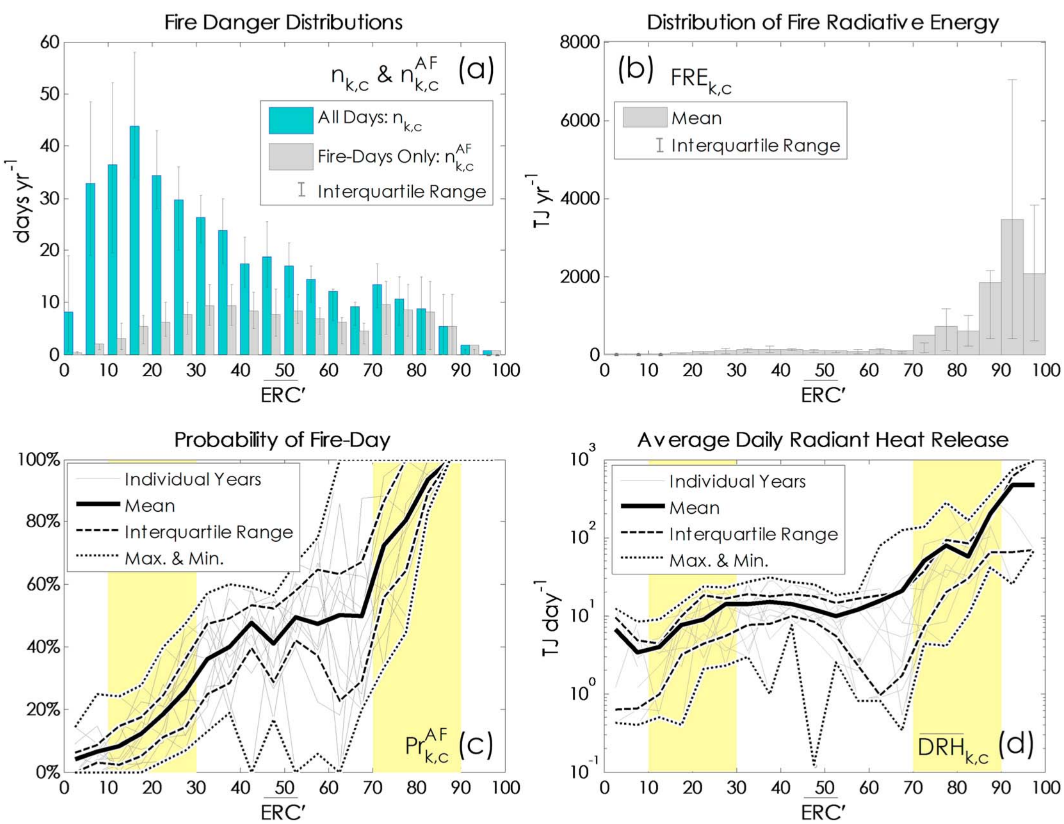

Figure 4. Graphical depiction of equation (6) for the North Central Rockies Forests (NCRFs) ecoregion, identified by the subscript k. (a) The fire danger distribution as a function of the Energy Release Component (ERC) for all days, $n_{k,c}$, alongside the fire danger distribution on fire days only when MODIS detects at least one active fire (AF) pixel. (b) The distribution of fire radiative energy (FRE) detected by MODIS as a function of ERC. (c) The probability curve $Pr^{AF}_{k,c}$ indicates the likelihood of MODIS detecting at least one AF pixel in the ecoregion as function of ERC. (d) The average radiant heat release per fire day, $\overline{DRH}_{k,c}$. Note the log scale in Figure 4d. The yellow bands centered at $\overline{ERC}' = 20$ and $\overline{ERC}' = 80$ illustrate the low and high fire danger intervals over which the ratios, ρ, are calculated (see Figure 5).

Nevertheless, the inherently low MODIS detection probability at low fire danger amounts to very little absolute difference between the two probability curves derived from the different burned area and active fire products (Figure 6). Similarly, the magnitudes of the two probability curves are nearly equivalent at high fire danger when both the MODIS burned area and active fire detection algorithms are equally capable of detecting the presumably larger and more intense wildland fires. At moderate fire danger conditions $\left(30 < \overline{ERC}' < 70\right)$, however, MODIS is more likely to detect an active fire pixel rather than a burned area pixel in almost every ecoregion across CONUS (Figure 6).

Ratios of daily burning characteristics observed by MODIS on days of high versus low fire danger also varied across CONUS (Figures 5c and 5d), suggesting regional differences in the response of existing wildland fires to changes in concurrent weather conditions. Technically, values of $\rho_{\overline{DBA}} > 1.0$ and $\rho_{\overline{DRH}} > 1.0$ indicate that MODIS detects greater areal fire growth and radiant heat release at higher fire danger. However, considering the caveats of the MODIS detection algorithms, it can be inferred that values of $\rho_{\overline{DBA}} > 1.0$ and $\rho_{\overline{DRH}} > 1.0$ indicate that landscape fires are either more numerous, larger, or burning more intensely during hotter, drier fire weather conditions. Similar to the probability curves, MODIS almost always detects more extreme fire behavior on days with higher fire danger compared to lower fire danger, with $\rho_{\overline{DBA}}$ and $\rho_{\overline{DRH}}$ exceeding 1.0 in ecoregions accounting for 87% and 99% of CONUS by area, respectively. Where over the course of 12 years numerous, large fires aligned with hot and dry conditions, there are substantial differences in the average daily burning characteristics observed by MODIS on days of high fire danger versus low fire danger, with $\rho_{\overline{DBA}}$ and $\rho_{\overline{DRH}}$ exceeding 5.0 across more than 42% of CONUS by area.

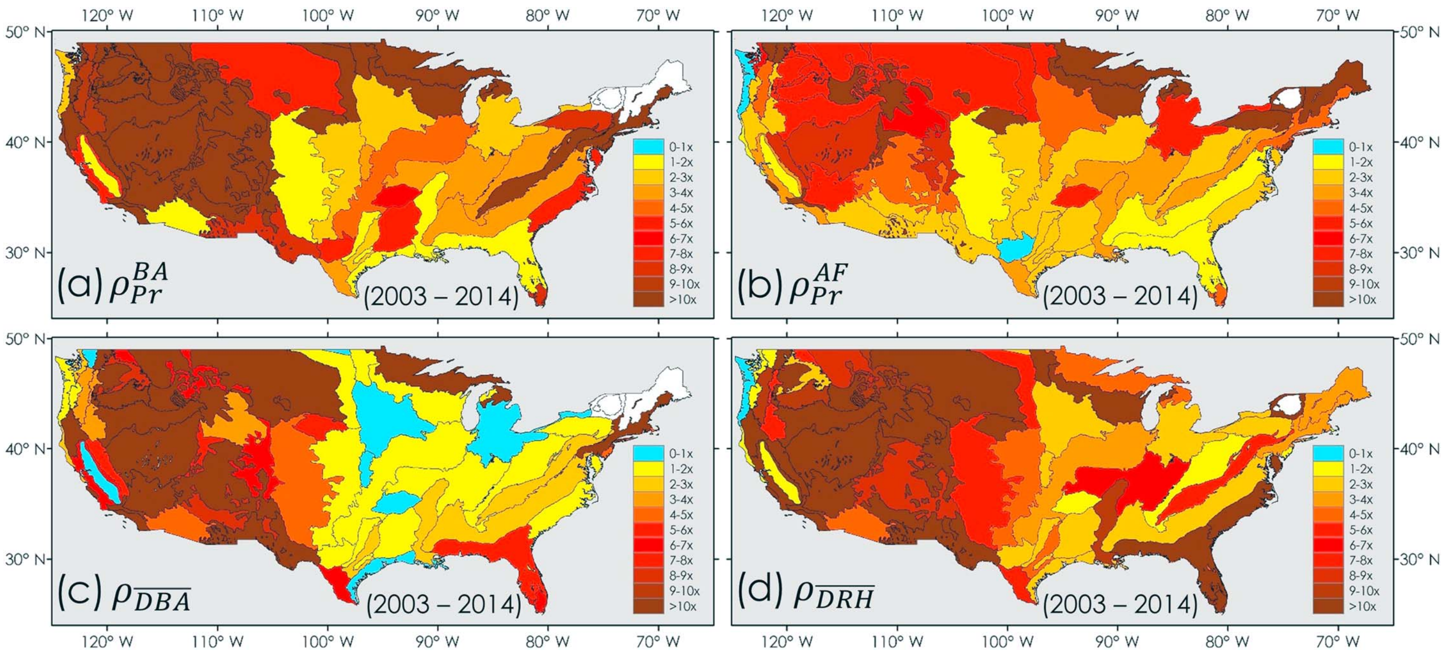

Figure 5. Ratios (ρ) of fire presence and burning characteristics observed by MODIS at high fire danger versus low fire danger. Ecoregions with values of (a) $\rho_{Pr}^{BA} > 1.0$ and (b) $\rho_{Pr}^{AF} > 1.0$ indicate that MODIS is more likely to detect a burned area (BA) pixel or an active fire (AF) pixel, respectively, on days with high fire danger. Ecoregions with values of (c) $\rho_{\overline{DBA}} > 1.0$ and (d) $\rho_{\overline{DRH}} > 1.0$ indicate that MODIS detects greater daily burned area (DBA) and daily radiant heat release (DRH) on days with high fire danger. Considering the caveats of the MODIS detection algorithms, these ratios illustrate (i) regional variations in the response of landscape fire activity to changes in fire danger and (ii) landscape fires across the majority of CONUS are more likely to be present and burning more vigorously during hotter, drier fire weather conditions.

5.1.3. Biome-Level Summaries

Hotter and drier conditions promote an increase in the amount of fuel consumed per unit area, and at the biome-level MODIS is capable of detecting an increase in fuel load reduction with increasing fire danger (Figure 7). The Temperate Coniferous Forests and the Mediterranean Forests, Woodlands, and Scrub biomes

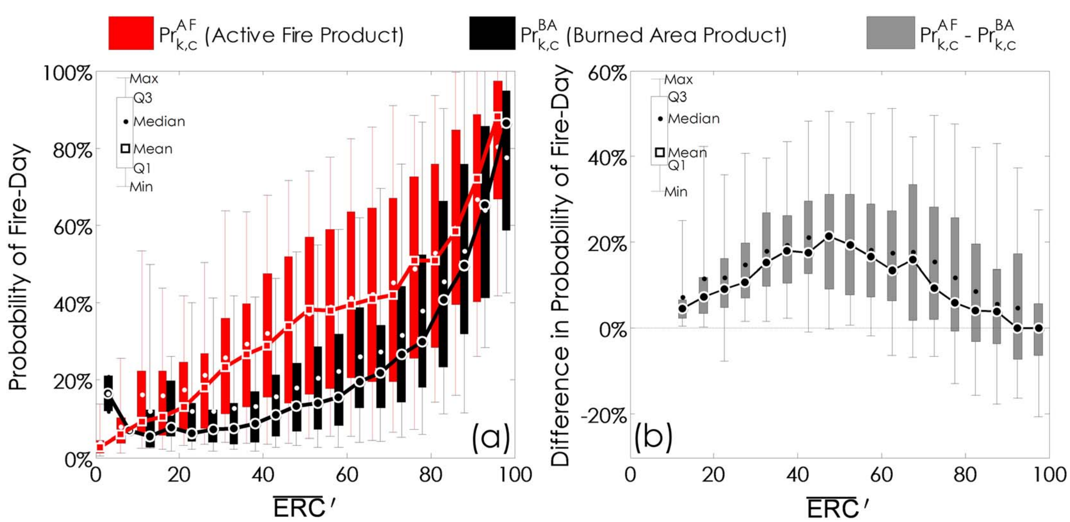

Figure 6. Summary of the probability curves generated for all 72 ecoregions across CONUS using the MODIS burned area (BA) and active fire (AF) products, $Pr_{k,c}^{BA}$ and $Pr_{k,c}^{AF}$, respectively. In general, (a) the probability of a fire day (i.e., a day when MODIS detects evidence of at least one wildland fire) increases as the Energy Release Component (ERC) increases, implying that landscape fires are more likely to be burning during hotter, drier fire weather conditions. (b) Due to differences in the detection algorithms, there is almost always a greater likelihood that MODIS will detect an active fire pixel compared to a burned area pixel, particularly on days with moderate fire danger conditions.

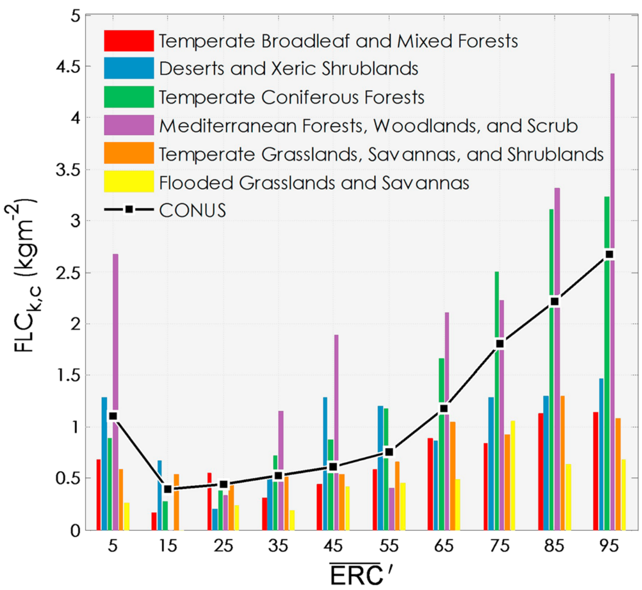

Figure 7. Relationships between fuel load consumption (FLC; kg m^{-2}) and the Energy Release Component (ERC) for six prominent biomes plus CONUS. Values of FLC are obtained by (i) intersecting daily ERC grids with spatially and temporally coincident MODIS burned area (MCD64A1) and active fire (MCD14ML) pixels from 2003 to 2014, (ii) converting estimates of fire radiative power (FRP) into fire radiative energy (FRE), and (iii) converting FRE into estimates of dry matter (DM) consumption.

exhibit the highest values of fuel load consumption and also exhibit the greatest sensitivity to changes in fire danger, as evidenced by the rapid increase in fuel load consumption when $\overline{ERC}' \geq 50$. These two biomes account for 41% of the coincident burned area and 65% of the coincident FRE detected by MODIS and are therefore mainly responsible for the CONUS-wide increase in fuel load consumption from low to high fire danger.

5.2. Annual Predictions From 1979 to 2014

5.2.1. The North Central Rockies Forests

Robust linear regressions fit to the mean annual predictions for the NCRF reveal that changes in fire danger from 1979 to 2014 have had the potential to induce a +540.6 ha yr^{-1} trend in burned area (Figure 8a), and a +51.1 TJ yr^{-1} trend in FRE, corresponding to a +0.02 Tg yr^{-1} trend in DM consumption (Figure 8b). Differences in the two empirical probability curves ($Pr^{BA}_{k,c}$ and $Pr^{AF}_{k,c}$) particularly at moderate fire danger conditions (Figure 6b) resulted in consistently shorter fire activity season lengths (FASLs) when predicted from the MODIS burned area (BA) product compared to the active fire (AF) product. Despite this bias, trends fit to both predictions of the fire activity season length reveal a nearly identical expansion in the NCRF: +0.65 d yr^{-1} (Figure 8c) versus +0.58 d yr^{-1} (Figure 8d). Relative increases in annual burned area and dry matter consumption in the NCRF outpaced the relative expansion of the fire activity season length. This resulted in positive trends in both the annual average daily burned area and the annual average daily heat release (Figures 7e and 7f). Thus, fire danger-induced trends in annual burned area and annual dry matter consumption in the NCRF can be attributed to both an increase in the number of days per year that fires are present on the landscape and an intensification of daily burning characteristics.

5.2.2. Ecoregion-Level Summaries

Changes in fire danger since 1979 have had the potential to induce significant ($\alpha = 0.05$) positive trends in annual burned area and annual dry matter consumption across 45–48% of CONUS, with the majority of the interior west exhibiting a more than doubling in the annual magnitude of biomass burning (Figures 9a and 9b). Increases in the annual magnitude of fire activity are partly attributed to an increase in the number of days per year that wildland fires are present on the landscape, with significant positive trends in the fire activity season length found in ecoregions accounting for 42–49% of the area of CONUS (Figures 9c and 9d). In many interior-western ecoregions, the rate of increase in annual burned area and dry matter consumption outpaced the expansion of the fire activity season length. Consequently, long-term changes in fire danger have had the potential to intensify daily burning characteristics across 37–45% of CONUS, as evidenced by significant positive trends in the annual average daily fire growth (Figures 9e) and annual average daily radiant heat release (Figure 9f).

5.2.3. Biome-Level Summaries

Results presented for seven biomes accounting for >99% of the dry matter consumed across CONUS indicate a mostly positive trend in fuel load consumption over the course of 36 years, though not all trends are significant at the 95% confidence level (Table 1). Of the biomes with significant trends, the Temperate Coniferous Forests (+17.1 g m^{-2} yr^{-1}) and the Mediterranean Forests, Woodlands, and Scrub (+39.1 g m^{-2} yr^{-1}) exhibited the greatest absolute increases in fuel load consumption, which is largely attributed to the dramatic response of wildland fires in these ecoregions when burning under hotter and drier conditions (Figure 7).

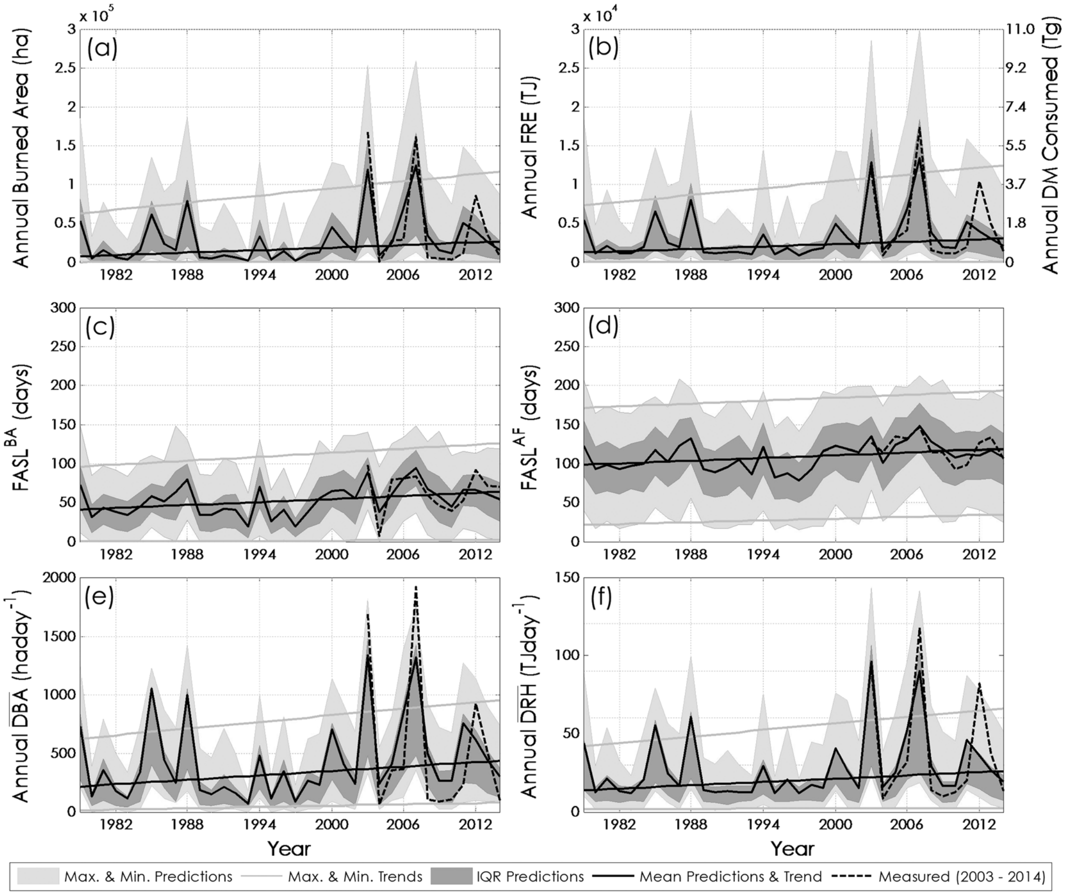

Figure 8. Predictions and trends in annual fire activity for the North Central Rockies Forests (NCRFs) ecoregion modeled solely based on changes in fire danger from 1979 to 2014. (a) Predictions of annual burned area (ha) and (b) annual fire radiative energy (FRE; MJ) and dry matter (DM; Tg) consumption. (c and d) Fire activity season lengths (FASL; days) are determined from the MODIS burned area (BA) and active fire (AF) products, respectively. (e and f) The annual average daily burned area $\left(\overline{\mathrm{DBA}}\right)$ and daily radiant heat release $\left(\overline{\mathrm{DRH}}\right)$. Robust linear regressions are used to characterize the trends which are mapped for every ecoregion across CONUS in Figure 9.

5.2.4. CONUS-Level Summaries

Predictions of annual burned area from equations (9) and (11) are strongly correlated (r=0.99), with CONUS-wide estimates from equation (11) being on average 1.36 Mha (95.6%) greater than from equation (9). This comparison demonstrates that leveraging the MODIS active fire product to predict burned area via equation (11) largely circumvents the relatively poorer performance of the MODIS burned area detection algorithm when used in isolation (Figure 6). Consequently, predictions of annual burned area from 1997 to 2014 obtained directly from equation (9) agree well with the annual burned area retrieved from the Global Fire Emissions Database (GFED) version 4.0 (Figure 10a), while estimates of annual DM consumption from equation (10), indirect estimates of annual burned area from equation (11), and estimates of the amount of fuel consumed per unit area agree better with the small fire boosted values [*Randerson et al.*, 2012] reported in GFED version 4.1s (Figures 10b–10d).

Overall, in the absence of any other influences on fire regimes, changes in fire danger since 1979 have had the potential to induce a CONUS-wide a +0.51 Tg yr^{-1} trend in DM consumption, which itself is driven by the combined effect of a +0.02 Mha yr^{-1} trend in burned area and a +10.6 g m^{-2} yr^{-1} trend in fuel load consumption (Table 1).

6. Discussion

This work leverages a well-known set of equations linking dry matter consumption with burned area, fuel load reduction, and heat release and then reformulates these equations as functions of the location and environmental conditions on the day of burning. Constructing bivariate relationships between fire danger,

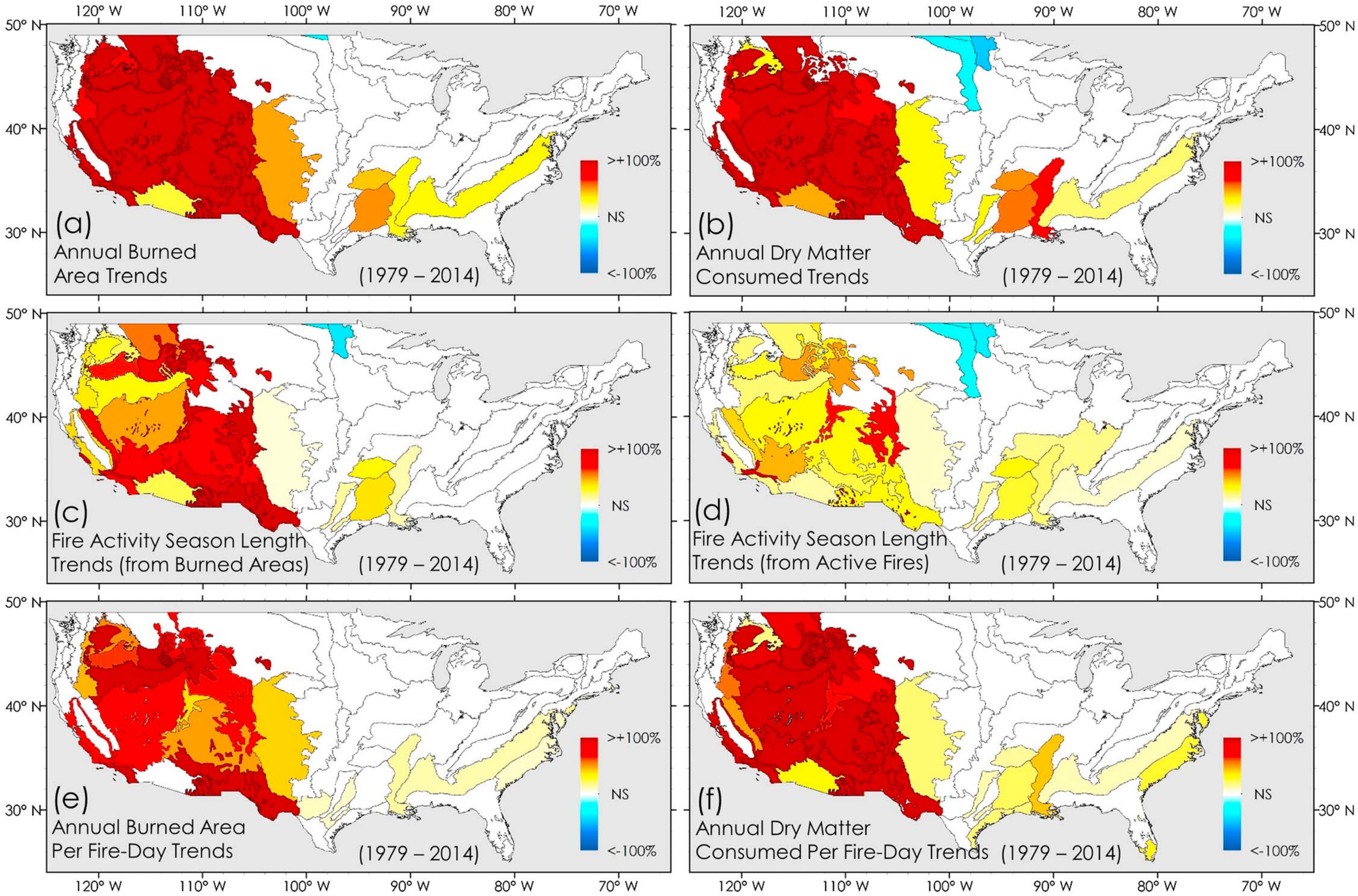

Figure 9. Relative changes (in percent) in ecoregion-level fire activity predicted solely from changes in fire danger from 1979 to 2014: (a) annual burned area, (b) annual dry matter consumed, (c and d) fire activity season lengths, (e) annual average daily burned area, and (f) annual average daily dry matter consumed. Trends in each ecoregion are based on robust linear regressions (e.g., see Figure 8), and trends that are not significant (NS) are not shown.

Table 1. Summary of Biome-Level and CONUS-Wide Trends in Annual Dry Matter (DM) Consumption, Annual Burned Area, and Annual Fuel Load Consumption (FLC) From 1979 to 2014[a]

Biome	Trend: Annual Burned Area Equation (9) ($ha yr^{-1}$)	Trend: Annual DM Consumed Equation (10) ($Tg yr^{-1}$)	Trend: Annual Burned Area Equation (11) ($ha yr^{-1}$)	Trend: Annual FLC Equations (10) and (11) ($g m^{-2} yr^{-1}$)
Temperate Broadleaf and Mixed Forests	+1,083.18 (±817.30)	+0.024 (±0.023)	+2,009.00 (±1,935.38)	+1.91 (±2.15)
Temperate Coniferous Forests	+8,614.27 (±5,178.43)	+0.262 (±0.165)	+9,031.49 (±5376.13)	+17.10 (±10.00)
Tropical and Subtropical Grasslands, Savannas, and Shrublands	+40.18 (±56.27)	0.004 (±0.004)	+176.80 (±196.30)	+3.96 (±4.36)
Temperate Grasslands, Savannas, and Shrublands	−25.47 (±3,494.62)	−0.002 (±0.038)	+345.05 (±5,057.13)	−0.03 (±1.38)
Flooded Grasslands and Savannas	−171.91 (±432.47)	+0.002 (±0.002)	+86.13 (±276.49)	+2.14 (±1.96)
Mediterranean Forests, Woodlands, and Scrub	+1,895.52 (±987.29)	+0.061 (±0.030)	+2,090.10 (±1,041.57)	+39.11 (±12.50)
Deserts and Xeric Shrublands	+8,672.28 (±4,050.52)	+0.101 (±0.048)	+7,426.12 (±3,459.68)	+6.15 (±2.99)
CONUS	+22,403.4 (±13,454.5)	+0.505 (±0.279)	+22,464.0 (±14,315.3)	+10.6 (±5.0)

[a]Annual burned area from equation (9) in column 1 is derived from the MODIS burned area product only, while annual burned area from equation (11) in column 3 is derived from a combination of the MODIS burned area and active fire products. Trends are based on robust linear regression models and include the 95% confidence interval (in parentheses).

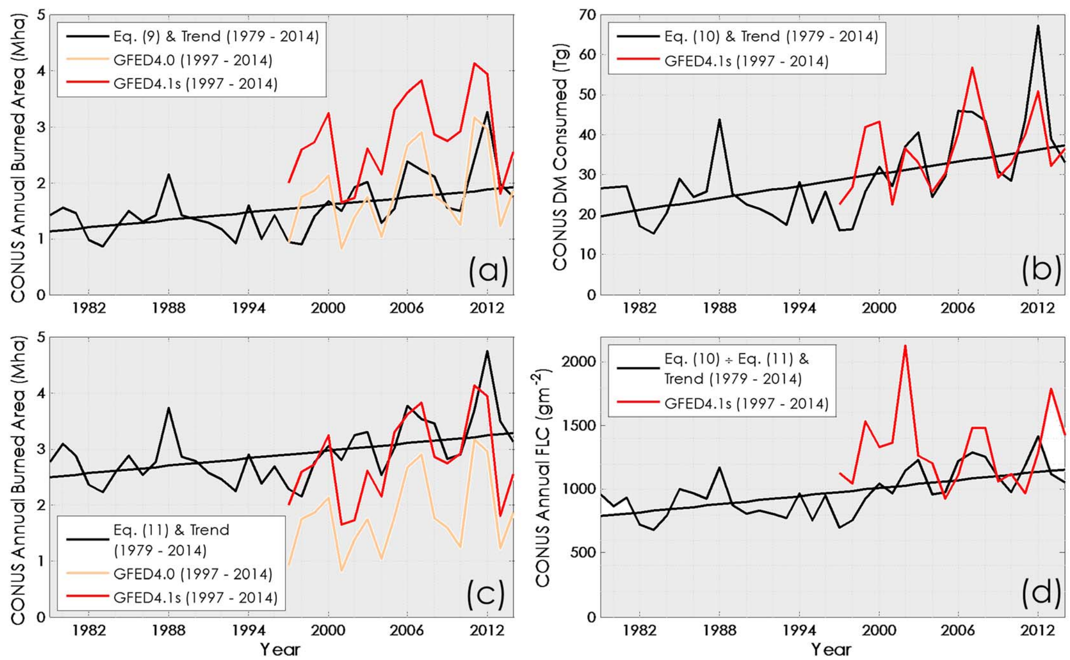

Figure 10. CONUS-wide comparisons between annual predictions developed herein (1979–2014) and the Global Fire Emissions Database (GFED) versions 4.0 and 4.1s (1997–2014). Whereas both versions of GFED [*van der Werf et al*., 2010] utilize the MODIS burned area (MCD64A1) product [*Giglio et al*., 2013], version 4.1s includes an estimate of the contribution from hot spots detected outside of burned areas [*Randerson et al*., 2012]. (a) Direct estimates of annual burned area (Mha) from equation (9). (b) Annual dry matter (DM; Tg) consumed from equation (10). (c) Indirect estimates of annual burned area from equation (11). (d) Fuel load consumption (FLC; kg m^{-2}) from equations (10) and (11). Trends based on robust linear regressions are reported in Table 1.

fire presence, and average daily burning characteristics (Figures 3 and 4) conveniently associates the regional response of wildland fires to changes in environmental conditions at the time of burning. Admittedly, however, the sole use of fire danger, and specifically the Energy Release Component (ERC), as an indicator of the weather and fuel moisture conditions concurrent with burning fails to fully capture all of the climatic and nonclimatic factors that influence fire activity. For example, the probability of at least one wildland fire burning in an ecoregion depends on several other factors besides ERCs that govern the timing and location of new ignitions (e.g., lightning flash characteristics, land management practices, recreational accidents, and malicious intent) as well as the persistence of existing fires (e.g., fuel continuity and suppression effectiveness). Although these underlying factors remain unaccounted for here, they are nevertheless inherent to the empirical probability curves and are particularly conspicuous on the occasions when fires are burning at very low fire danger, suggesting that other factors (such as agricultural or other prescribed burning practices) can facilitate the ignition and propagation of wildland fires despite unfavorable weather and fuel moisture conditions. Limiting factors besides ERCs also affect daily burning characteristics. On days with the same ERC, for example, more area will burn and more fuel will be consumed if there are higher wind speeds or if there are a greater number of larger fires burning on the landscape, neither of which are explicitly accounted for in the simplified relationship between ERCs and daily burning characteristics. As such, other unmeasured, limiting factors besides ERCs are likely contributing to the year-to-year variations in the empirical functions.

The MODIS coverage and resolution coincides well with the spatiotemporal intent of the U.S. National Fire Danger Rating System (USNFDRS). However, as with agency fire records, the MODIS fire products suffer from spatial and temporal limitations that must be understood before the response of MODIS can be linked with the response of true fire activity. The MODIS-derived relationships between fire danger and fire activity presented here agree well with results presented for a nearby Predictive Service Area in the Northern Rockies based upon Remote Automated Weather Station (RAWS) data and agency fire reports [*Freeborn et al*., 2015]. However, the degree of such agreements is expected to vary regionally since the efficacy of the empirical functions developed herein hinges on the MODIS detection performance, which varies depending on fire type, canopy cover, atmospheric conditions, and sensor viewing geometry [*Csiszar et al*., 2006; *Morisette et al*., 2005; *Schroeder et al*., 2008]. Ultimately, failed and false detections affect the ability of MODIS to record fire days and to estimate the true burned area [*Mangeon et al*., 2015] and fire radiative power [*Peterson et al*., 2013]. Somewhat reassuringly, however, empirical functions are constructed here by accumulating numerous pixels over large areas and on multiple days within fairly wide intervals of fire danger, thereby partially mitigating uncertainties in MODIS observations collected on a per pixel and instantaneous basis [*Freeborn et al*., 2014].

Despite ERC's limitations as the sole indicator of in-season environmental conditions, and the caveats surrounding the ability of the MODIS fire products to depict the true fire activity, the empirical functions developed herein reveal regional differences in the response of fire activity to changes in coincident weather and fuel moisture conditions. These empirical functions cannot be considered as unique, ecoregion-specific signatures since, as of yet, it is unclear whether these relationships change over time. Changes in the shape or magnitude of these functions over time would imply that changes in vegetation types or ignition patterns cause a shift in the response of fire activity to in-season weather and fuel moisture conditions. Temporal shifts in the empirical functions cannot be ascertained here due to the brief MODIS era (2003–2014) and interannual fluctuations in fire weather and fire activity. However, since the empirical functions vary geographically (Figure 5), it is fully expected that relationships between fire danger and fire activity should also vary over time.

Although bivariate relationships may fail to account for all of the climatic and nonclimatic factors that influence fire activity, the empirical functions developed here enable annual fire activity to be predicted either retrospectively or for future scenarios using only a fire danger climatology. Applying the modern empirical functions to the entire 36 year climatology assumes that relationships between fire danger and fire activity remain unaffected by concurrent, long-term changes in vegetation types or ignition patterns. Thus, the ecoregion, biome, and continental trends presented here reflect the isolated impact of changing fire weather conditions on annual fire activity. In reality, however, the fire chronologies and characteristics reconstructed here are either intensified or dampened by concurrent—though unaccounted for—changes in vegetation fuel types and densities, ignition patterns, and land use and land management practices.

In equations 9–11, uncertainties in the relationships between fire danger, fire presence, and daily burning characteristics induce uncertainties in the prediction of annual fire activity. Regrettably, we have not propagated the individual uncertainties through our model to ascertain their relative impacts on the annual predictions. Future uncertainty analyses could be used to identify which parameters require more accurate estimates and could also be used to identify regions where relationships between fire danger and fire activity are most stable, compared to those regions where uncertainty in the relationships is strongly affected by interannual fluctuations in fuel availability or ignition patterns.

Ultimately, this work quantifies the magnitude of fire activity in terms beyond the annual burned area. In our formulations, annual burned area is determined by the fire activity season length (FASL), or the number of days that fires are present on the landscape, and the average daily fire growth rate. Though forthcoming, we have not performed a sensitivity analysis to determine whether the FASL or the average daily burning characteristic is the main driver of burned area in each ecoregion. As in *Seiler and Crutzen* [1980], annual dry matter consumption is determined by annual burned area and fuel load reduction. In the future we intend to identify whether an increase in annual burned area or an increase in fuel load consumption is the more influential factor driving the biome-level trends in annual dry matter consumption. Verifying the accuracies and uncertainties of either satellite-derived or modeled estimates of fuel load consumption, however, is hindered by a rarity of field measurements [*van Leeuwen et al*., 2014]. Nevertheless, if it assumed that the preburn fuel load is constant during the weeks or months when wildland fires are present, then seasonal fluctuations in the amount of fuel consumed per unit area can solely be attributed to the influence of changing weather conditions on consumption completeness.

Agreement between predictions of annual burned area obtained directly from equation (9) and values retrieved from the Global Fire Emissions Database (GFED) version 4.0, as well as the agreement between our CONUS-wide +0.022 Mha yr^{-1} trend in annual burned area and a MODIS era trend (2000–2012) of +0.02 Mha yr^{-1} reported by *Giglio et al*. [2013], is not surprising since the MODIS direct broadcast (MCD64A1) burned area product serves as the basis for these estimates. Reassuringly, our predictions of annual burned area obtained indirectly from equation (11), which is designed to mitigate differences between the MODIS burned area and active fire detection performance, agree well with GFED 4.1s, which itself includes a small fire boost [*Randerson et al*., 2012]. The agreement between our predictions of annual

DM consumption and values reported in GFED version 4.1s is somewhat surprising given (i) the application of a small fire boost [*Randerson et al.*, 2012] and (ii) estimates of fuel consumption obtained from active fire observations are generally lower than those obtained from burned area observations [*Ellicott et al.*, 2009]. It can only be surmised that our close agreement here with GFED4.1s is likely attributed to the constant of proportionality used to convert FRP summations to FRE.

7. Conclusion

The wide ground swath and frequent overpass schedule of MODIS is well suited to provide wildland fire observations that can be aligned with fire danger indices at spatiotemporal scales for which the U.S. National Fire Danger Rating System is intended. The ability of MODIS to detect fire presence and quantify the magnitude of regional fire activity on a daily basis offers additional information not found in agency fire reports and enables annual fire statistics to be decomposed into previously unquantifiable attributes, such as seasonal duration, average daily fire growth, average daily heat release, and fuel load consumption. Synchronizing spatially resolved fire danger indices with MODIS fire observations offers opportunities to associate environmental conditions with concurrent wildland fire activity, and the application of modern associations provides a pathway for predicting changes in coarse-scale fire occurrence and burning characteristics solely from changes in fire danger. Although empirical functions relating fire danger with fire activity can help elucidate at least one facet of climate-fire relationships, it must be admitted that the sole use of ERCs—as a proxy for fuel moisture contents—fails to fully capture all of the climatic and nonclimatic factors that affect the ignition and propagation of wildland fires. Likewise, the efficacy of the empirical functions and annual predictions developed herein hinges on the ability of the MODIS fire products to accurately represent the true fire activity. Nevertheless, results reveal regional variations in the response of wildland fires to changes in fire danger and that weather conditions concurrent with burning have a three-pronged impact on the magnitude of annual fire activity by affecting the seasonal duration, spatial extent, and combustion intensity.

Appendix A

The appendix consists of Table A1 which summarizes the notation, terminology, and equations used in this work.

Table A1. Summary of Notation, Terminology, and Equations Used in this Work

Ecoregion or biome identifier	subscript k	A1
Fire danger interval; equal-width bins of normalized mean Energy Release Component (ERC)	subscript c=1,2, …, 20	A2
Burned area product (MCD64A1) identifier	superscript BA	A3
Active fire product (MCD14ML) identifier	superscript AF	A4
Fire danger distribution; number of days within fire danger interval	$n_{k,c}$	A5
Fire danger distribution on fire days only; number of fire days within fire danger interval	$n^{BA}_{k,c}$ or $n^{AF}_{k,c}$	A6
Probability of a fire day	$\mathrm{Pr}^{BA}_{k,c} = \frac{n^{BA}_{k,c}}{n_{k,c}}$	A7
Probability of a fire day	$\mathrm{Pr}^{AF}_{k,c} = \frac{n^{AF}_{k,c}}{n_{k,c}}$	A8
Ratio of probability of a fire day at high fire danger versus low fire danger	$\rho^{BA}_{\mathrm{Pr}} = \frac{\mathrm{Pr}^{BA}_{k,15\le c\le 18}}{\mathrm{Pr}^{BA}_{k,3\le c\le 6}}$	A9
Ratio of probability of a fire day at high fire danger versus low fire danger	$\rho^{AF}_{\mathrm{Pr}} = \frac{\mathrm{Pr}^{AF}_{k,15\le c\le 18}}{\mathrm{Pr}^{AF}_{k,3\le c\le 6}}$	A10
Total burned area (TBA) in fire danger interval	$\mathrm{TBA}_{k,c}$	A11
Average daily burned area (DBA) in fire danger interval	$\overline{\mathrm{DBA}}_{k,c} = \frac{\mathrm{TBA}_{k,c}}{n^{BA}_{k,c}}$	A12
Fire radiative energy (FRE) detected in fire danger interval	$\mathrm{FRE}_{k,c}$	A13
Average daily radiant heat release (DRH) detected in fire danger interval	$\overline{\mathrm{DRH}}_{k,c} = \frac{\mathrm{FRE}_{k,c}}{n^{AF}_{k,c}}$	A14
Ratio of average daily burned area (DBA) at high fire danger versus low fire danger	$\rho_{\overline{\mathrm{DBA}}} = \frac{\overline{\mathrm{DBA}}_{k,15\le c\le 18}}{\overline{\mathrm{DBA}}_{k,3\le c\le 6}}$	A15
Ratio of average daily radiant heat release (DRH) at high fire danger versus low fire danger	$\rho_{\overline{\mathrm{DRH}}} = \frac{\overline{\mathrm{DRH}}_{k,15\le c\le 18}}{\overline{\mathrm{DRH}}_{k,3\le c\le 6}}$	A16
Fire activity season length (FASL); number of days per year that MODIS is expected to detect at least one burned area pixel	$\mathrm{FASL}^{BA}_{k,yr} = \sum_{c=1}^{20} n_{k,c,yr} \times \mathrm{Pr}^{BA}_{k,c}$	A17
Fire activity season length (FASL); number of days per year that MODIS is expected to detect at least one active fire pixel	$\mathrm{FASL}^{AF}_{k,yr} = \sum_{c=1}^{20} n_{k,c,yr} \times \mathrm{Pr}^{AF}_{k,c}$	A18

Acknowledgments
Funding is provided by NASA grants NNH11ZDA001N-FIRES, NNX11AB89G, and NNX12AQ88G. Thanks to those maintaining the University of Maryland ftp server (fuoco.geog.umd.edu) for hosting the MODIS direct broadcast (DB) burned area (MCD64A1) and global fire location (MCD14ML) products. Thanks also to the two reviewers and the Editor for their time and very constructive comments that have no doubt improved the final version of this manuscript.

References

Abatzoglou, J. T. (2013), Development of gridded surface meteorological data for ecological applications and modelling, *Int. J. Climatol.*, *33*(1), 121–131.

Abatzoglou, J. T., and C. A. Kolden (2011), Relative importance of weather and climate on wildfire growth in interior Alaska, *Int. J. Wildland Fire*, *20*(4), 479–486.

Abatzoglou, J. T., and C. A. Kolden (2013), Relationships between climate and macroscale area burned in the western United States, *Int. J. Wildland Fire*, *22*(7), 1003–1020.

Andela, N., G. R. van der Werf, J. Kaiser, T. T. van Leeuwen, M. J. Wooster, and C. E. R. Lehmann (2016), Biomass burning fuel consumption dynamics in the tropics and subtropics assessed from satellite, *Biogeosciences*, *13*(12), 3717–3734.

Anderson, H. E. (1969), Heat transfer and fire spread, *Res. Pap. INT-RP-69*, 20 pp., USDA For. Serv., Intermt. For. and Range Exp. Stn.

Bachelet, D., R. P. Neilson, J. M. Lenihan, and R. J. Drapek (2001), Climate change effects on vegetation distribution and carbon budget in the United States, *Ecosystems*, *4*(3), 164–185.

Barbero, R., J. T. Abatzoglou, E. A. Steel, and N. K. Larkin (2014), Modeling very large-fire occurrences over the continental United States from weather and climate forcing, *Environ. Res. Lett.*, *9*(12), 124009.

Bradshaw, L. S., J. E. Deeming, R. E. Burgan, and J. D. Cohen (1983), The 1978 NFDRS: Technical documentation, *Gen. Tech. Rep. INT-169*, 44 pp., USDA For. Serv.

Burgan, R. E., R. W. Klaver, and J. M. Klaver (1998), Fuel models and fire potential from satellite and surface observations, *Int. J. Wildland Fire*, *8*(3), 159–170.

Csiszar, I., J. Morisette, and L. Giglio (2006), Validation of active fire detection from moderate-resolution satellite sensors: The MODIS example in northern Eurasia, *IEEE Trans. Geosci. Remote Sens.*, *44*, 1757–1764.

Daly, C., M. Halbleib, J. I. Smith, W. P. Gibson, M. K. Doggett, G. H. Taylor, J. Curtis, and P. P. Pasteris (2008), Physiographically sensitive mapping of climatological temperature and precipitation across the conterminous United States, *Int. J. Climatol.*, *28*(15), 2031–2064.

Deeming, J. E., R. E. Burgan, and J. D. Cohen (1977), The National Fire-Danger Rating System—1978, Rep., 63 pp., For. Serv., U.S. Dep. of Agric., Intermt. For. and Range Exp. Stn., Ogden, Utah.

de Groot, W. J., J. G. Goldammer, T. Keenan, M. A. Brady, T. J. Lynham, C. O. Justice, I. A. Csiszar, and K. O'Loughlin (2006), Developing a global early warning system for wildland fire, in *Proceedings of the V International Conference on Forest Fire Research*, edited by D. X. Viegas, 12 p., Elsevier, Amsterdam.

Dickinson, M. B., et al. (2016), Measuring radiant emissions from entire prescribed fires with ground, airborne and satellite sensors—RxCADRE 2012, *Int. J. Wildland Fire*, *25*(1), 48–61.

Dymond, C. C., R. D. Field, O. Roswintiarti, and Guswanto (2005), Using satellite fire detection to calibrate components of the Fire Weather Index system in Malaysia and Indonesia, *Environ. Manage.*, *35*(4), 426–440.

Eidenshenk, J., B. Schwind, K. Brewer, Z. Zhu, B. Quayle, and S. Howard (2007), A project for monitoring trends in burn severity, *Fire Ecol.*, *3*(1), 3–21.

Ellicott, E., E. Vermote, L. Giglio, and G. Roberts (2009), Estimating biomass consumed from fire using MODIS FRE, *Geophys. Res. Lett.*, *36*, L13401, doi:10.1029/2009GL038581.

Finney, M. A. (2005), The challenge of quantitative risk analysis for wildland fire, *For. Ecol. Manage.*, *211*(1–2), 97–108.

Finney, M. A., C. W. McHugh, I. C. Grenfell, K. L. Riley, and K. C. Short (2011), A simulation of probabilistic wildfire risk components for the continental United States, *Stochastic Environ. REs. Risk Assess.*, *25*(7), 973–1000.

Freeborn, P. H., M. J. Wooster, W. M. Hao, C. A. Ryan, B. L. Nordgren, S. P. Baker, and C. Ichoku (2008), Relationships between energy release, fuel mass loss, and trace gas and aerosol emissions during laboratory biomass fires, *J. Geophys. Res.*, *113*, D01301, doi:10.1029/2007JD008679.

Freeborn, P. H., M. J. Wooster, and G. Roberts (2011), Addressing the spatiotemporal sampling design of MODIS to provide estimates of the fire radiative energy emitted from Africa, *Remote Sens. Environ.*, *115*(2), 475–489.

Freeborn, P. H., M. J. Wooster, D. P. Roy, and M. A. Cochrane (2014), Quantification of MODIS fire radiative power (FRP) measurement uncertainty for use in satellite-based active fire characterization and biomass burning estimation, *Geophys. Res. Lett.*, *41*, 1988–1994, doi:10.1002/2013GL059086.

Freeborn, P. H., M. A. Cochrane, and W. M. Jolly (2015), Relationships between fire danger and the daily number and daily growth of active incidents burning in the northern Rocky Mountains, USA, *Int. J. Wildland Fire*, *24*(7), 900–910.

Gedalof, Z., D. L. Peterson, and N. J. Mantua (2005), Atmospheric, climatic, and ecological controls on extreme wildfire years in the northwestern United States, *Ecol. Appl.*, *15*(1), 154–174.

Giglio, L., J. Descloitres, C. O. Justice, and Y. J. Kaufman (2003), An enhanced contextual fire detection algorithm for MODIS, *Remote Sens. Environ.*, *87*(2–3), 273–282.

Giglio, L., T. Loboda, D. P. Roy, B. Quayle, and C. O. Justice (2009), An active-fire based burned area mapping algorithm for the MODIS sensor, *Remote Sens. Environ.*, *113*(2), 408–420.

Giglio, L., J. T. Randerson, and G. R. van der Werf (2013), Analysis of daily, monthly, and annual burned area using the fourth-generation Global Fire Emissions Database (GFED4), *J. Geophys. Res. Biogeosci.*, *118*, 317–328, doi:10.1002/jgrg.20042.

Giglio, L., W. Schroeder, and C. O. Justice (2016), The collection 6 MODIS active fire detection algorithm and fire products, *Remote Sens. Environ.*, *178*, 31–41.

Goldammer, J. G., and C. Price (1998), Potential impacts of climate change on fire regimes in the tropics based on MAGICC and a GISS GCM-derived lightning model, *Clim. Change*, *39*(2–3), 273–296.

Grissino-Mayer, H. D., and T. W. Swetnam (2000), Century-scale climate forcing of fire regimes in the American Southwest, *Holocene*, *10*(2), 213–220.

Heyerdahl, E. K., L. B. Brubaker, and J. K. Agee (2001), Spatial controls of historical fire regimes: A multiscale example from the interior west, USA, *Ecology*, *82*(3), 660–678.

Heyerdahl, E. K., L. B. Brubaker, and J. K. Agee (2002), Annual and decadal climate forcing of historical fire regimes in the interior Pacific Northwest, USA, *Holocene*, *12*(5), 597–604.

Hurteau, M. D., and M. L. Brooks (2011), Short- and long-term effects of fire on carbon in US dry temperate forest systems, *BioScience*, *61*(2), 139–146.

Hurteau, M. D., J. B. Bradford, P. Z. Fule, A. H. Taylor, and K. L. Martin (2014), Climate change, fire management, and ecological services in the southwestern US, *For. Ecol. Manage.*, *327*, 280–289.

Ichoku, C., and Y. J. Kaufman (2005), A method to derive smoke emission rates from MODIS fire radiative energy measurements, *IEEE Trans. Geosci. Remote Sens.*, *43*(11), 2636–2649.

Jolly, W. M., M. A. Cochrane, P. H. Freeborn, Z. A. Holden, T. J. Brown, G. J. Williamson, and D. M. J. S. Bowman (2015), Climate-induced variations in global wildfire danger from 1979 to 2013, *Nat. Commun.*, *6*, 7537.

Justice, C. O., L. Giglio, S. Korontzi, J. Owens, J. T. Morisette, D. Roy, J. Descloitres, S. Alleaume, F. Petitcolin, and Y. Kaufman (2002), The MODIS fire products, *Remote Sens. Environ.*, *83*(1–2), 244–262.

Kaiser, J. W., et al. (2012), Biomass burning emissions estimated with a global fire assimilation system based on observed fire radiative power, *Biogeosciences*, *9*(1), 527–554.

Kashian, D. M., W. H. Romme, D. B. Tinker, M. G. Turner, and M. G. Ryan (2006), Carbon storage on landscapes with stand-replacing fires, *BioScience*, *56*(7), 598–606.

Kauffman, J. B., and R. E. Martin (1989), Fire behavior, fuel consumption, and forest-floor changes following prescribed understory fires in Sierra-Nevada mixed conifer forests, *Can. J. For. Res.*, *19*(4), 455–462.

Kaufman, Y., C. Justice, L. Flynn, J. Kendall, E. Prins, L. Giglio, D. Ward, W. Menzel, and A. Setzer (1998), Potential global fire monitoring from EOS-MODIS, *J. Geophys. Res.*, *103*, 32,215–32,238, doi:10.1029/98JD01644.

Keane, R. E., G. J. Cary, I. D. Davies, M. D. Flannigan, R. H. Gardner, S. Lavorel, J. M. Lenihan, C. Li, and T. S. Rupp (2004), A classification of landscape fire succession models: Spatial simulations of fire and vegetation dynamics, *Ecol. Modell.*, *179*(1), 3–27.

Keane, R. E., P. F. Hessburg, P. B. Landres, and F. J. Swanson (2009), The use of historical range and variability (HRV) in landscape management, *For. Ecol. Manage.*, *258*(7), 1025–1037.

Keeley, J. E., G. H. Aplet, N. L. Christensen, S. G. Conard, E. A. Johnson, P. N. Omi, D. L. Peterson, and T. W. Swetnam (2009), Ecological foundations for fire management in North American forest and shrubland ecosystems, Rep., 92 pp., U.S. Dep. of Agric., For. Serv., Pac. Northwest Res. Stn., Portland, Oreg.

Knapp, E. E., J. E. Keeley, E. A. Ballenger, and T. J. Brennan (2005), Fuel reduction and coarse woody debris dynamics with early season and late season prescribed fire in a Sierra Nevada mixed conifer forest, *For. Ecol. Manage.*, *208*(1–3), 383–397.

Krause, A., S. Kloster, S. Wilkenskjeld, and H. Paeth (2014), The sensitivity of global wildfires to simulated past, present, and future lightning frequency, *J. Geophys. Res. Biogeosci.*, *119*, 312–322, doi:10.1002/2013JG002502.

Kremens, R. L., M. B. Dickinson, and A. S. Bova (2012), Radiant flux density, energy density and fuel consumption in mixed-oak forest surface fires, *Int. J. Wildland Fire*, *21*(6), 722–730.

Kumar, S. S., D. P. Roy, L. Boschetti, and R. Kremens (2011), Exploiting the power law distribution properties of satellite fire radiative power retrievals: A method to estimate fire radiative energy and biomass burned from sparse satellite observations, *J. Geophys. Res.*, *116*, D19303, doi:10.1029/2011JD015676.

Larkin, N. K., S. M. O'Neill, R. Solomon, S. Raffuse, T. Strand, D. C. Sullivan, C. Krull, M. Rorig, J. L. Peterson, and S. A. Ferguson (2009), The BlueSky smoke modeling framework, *Int. J. Wildland Fire*, *18*(8), 906–920.

Leenhouts, B. (1998), Assessment of biomass burning in the conterminous United States, *Conserv. Ecol.*, *2*(1), 1.

Littell, J. S., D. McKenzie, D. L. Peterson, and A. L. Westerling (2009), Climate and wildfire area burned in western U.S. ecoprovinces, 1916–2003, *Ecol. Appl.*, *19*(4), 1003–1021.

Liu, Y. Q., S. Goodrick, and W. Heilman (2014), Wildland fire emissions, carbon, and climate: Wildfire-climate interactions, *For. Ecol. Manage.*, *317*, 80–96.

Mangeon, S., R. Field, M. Fromm, C. McHugh, and A. Voulgarakis (2015), Satellite versus ground-based estimates of burned area: A comparison between MODIS based burned area and fire agency reports over North America in 2007, *Anthropocene Rev.*, *3*, 76–92.

Marlon, J. R., et al. (2012), Long-term perspective on wildfires in the western USA, *Proc. Natl. Acad. Sci. U.S.A.*, *109*(9), E535–E543, doi:10.1073/pnas.1112839109.

Miller, J. D., H. D. Safford, M. Crimmins, and A. E. Thode (2009), Quantitative evidence for increasing forest fire severity in the Sierra Nevada and Southern Cascade Mountains, California and Nevada, USA, *Ecosystems*, *12*(1), 16–32.

Mitchell, K. E., et al. (2004), The multi-institution North American Land Data Assimilation System (NLDAS): Utilizing multiple GCIP products and partners in a continental distributed hydrological modeling system, *J. Geophys. Res.*, *109*, D07S90, doi:10.1029/2003JD003823.

Morisette, J., L. Giglio, I. Csiszar, and C. Justice (2005), Validation of the MODIS active fire product over Southern Africa with ASTER data, *Int. J. Remote Sens.*, *109*, 4239–4264.

Nelson, R. M. (2000), Prediction of diurnal change in 10-h fuel stick moisture content, *Can. J. For. Res.*, *30*(7), 1071–1087.

Noble, I. R., A. M. Gill, and G. A. V. Bary (1980), McArthur's fire-danger meters expressed as equations, *Aust. J. Ecol.*, *5*, 201–203.

Nowacki, G. J., and M. D. Abrams (2008), The demise of fire and "mesophication" of forests in the eastern United States, *BioScience*, *58*(2), 123–138.

Olson, D. M., et al. (2001), Terrestrial ecoregions of the world: A new map of life on Earth, *BioScience*, *51*(11), 933–938.

Peterson, D., J. Wang, C. Ichoku, E. Hyer, and V. Ambrosia (2013), A sub-pixel-based calculation of fire radiative power from MODIS observations: 1. Algorithm development and initial assessment, *Remote Sens. Environ.*, *129*, 262–279.

Podur, J., and B. M. Wotton (2011), Defining fire spread event days for fire-growth modelling, *Int. J. Wildland Fire*, *20*(4), 497–507.

Price, C., and D. Rind (1994), Modeling global lightning distributions in a general-circulation model, *Mon. Weather Rev.*, *122*(8), 1930–1939.

Randerson, J. T., Y. Chen, G. R. van der Werf, B. M. Rogers, and D. C. Morton (2012), Global burned area and biomass burning emissions from small fires, *J. Geophys. Res.*, *117*, G04012, doi:10.1029/2012JG002128.

Reeves, M. C., K. C. Ryan, M. G. Rollins, and T. G. Thompson (2009), Spatial fuel data products of the LANDFIRE project, *Int. J. Wildland Fire*, *18*(3), 250–267.

Riley, K. L., J. T. Abatzoglou, I. C. Grenfell, A. E. Klene, and F. A. Heinsch (2013), The relationship of large fire occurrence with drought and fire danger indices in the western USA, 1984–2008: The role of temporal scale, *Int. J. Wildland Fire*, *22*(7), 894–909.

Roberts, G., M. Wooster, P. H. Freeborn, and W. Xu (2011), Integration of geostationary FRP and polar-orbiter burned area datasets for an enhanced biomass burning inventory, *Remote Sens. Environ.*, *115*(8), 2047–2061.

Rocca, M. E., P. M. Brown, L. H. MacDonald, and C. M. Carrico (2014), Climate change impacts on fire regimes and key ecosystem services in Rocky Mountain forests, *For. Ecol. Manage.*, *327*, 290–305.

Rothermel, R. C. (1972), A mathematical model for predicting fire spread in wildland fuels, Res. Pap. INT-115, 40 pp., USDA For. Serv., Intermt. For. and Range Exp. Stn.

Schoennagel, T., T. T. Veblen, and W. H. Romme (2004), The interaction of fire, fuels, and climate across Rocky Mountain forests, *BioScience*, *54*(7), 661–676.

Schroeder, W., E. Prins, L. Giglio, I. Csiszar, C. Schmidt, J. Morisette, and D. Morton (2008), Validation of GOES and MODIS active fire detection products using ASTER and ETM plus data, *Remote Sens. Environ.*, *112*, 2711–2726.

Seiler, W., and P. J. Crutzen (1980), Estimates of gross and net fluxes of carbon between the biosphere and the atmosphere from biomass burning, *Clim. Change*, *2*(3), 207–247.

Short, K. C. (2014), A spatial database of wildfires in the United States, 1992–2011, *Earth Syst. Sci. Data*, *6*(1), 1–27.

Slocum, M. G., W. J. Platt, and H. C. Cooley (2003), Effects of differences in prescribed fire regimes on patchiness and intensity of fires in subtropical savannas of Everglades National Park, Florida, *Restor. Ecol.*, *11*(1), 91–102.

Smith, A. M. S., W. T. Tinkham, D. P. Roy, L. Boschetti, R. L. Kremens, S. S. Kumar, A. M. Sparks, and M. J. Falkowski (2013), Quantification of fuel moisture effects on biomass consumed derived from fire radiative energy retrievals, *Geophys. Res. Lett.*, *40*, 6298–6302, doi:10.1002/2013GL058232.

Stephens, S. L., and L. W. Ruth (2005), Federal forest-fire policy in the United States, *Ecol. Appl.*, *15*(2), 532–542.

Theobald, D. M., and W. H. Romme (2007), Expansion of the US wildland-urban interface, *Landscape Urban Plann.*, *83*(4), 340–354.

Trouet, V., A. Taylor, A. Carleton, and C. Skinner (2009), Interannual variations in fire weather, fire extent, and synoptic-scale circulation patterns in northern California and Oregon, *Theor. Appl. Climatol.*, *95*(3–4), 349–360.

Urbanski, S. P., W. M. Hao, and B. Nordgren (2011), The wildland fire emission inventory: Western United States emission estimates and an evaluation of uncertainty, *Atmos. Chem. Phys.*, *11*(24), 12,973–13,000.

U.S. Environmental Protection Agency (2016), Inventory of U.S. greenhouse gas emissions and sinks: 1990–2014, *EPA 430-R-16-002*, 558 pp., U.S. Environ. Prot. Agency.

van der Werf, G. R., J. T. Randerson, L. Giglio, G. J. Collatz, M. Mu, P. S. Kasibhatla, D. C. Morton, R. S. DeFries, Y. Jin, and T. T. van Leeuwen (2010), Global fire emissions and the contribution of deforestation, savanna, forest, agricultural, and peat fires (1997–2009), *Atmos. Chem. Phys.*, *10*(23), 11,707–11,735.

van Leeuwen, T. T., et al. (2014), Biomass burning fuel consumption rates: A field measurement database, *Biogeosciences*, *11*(24), 7305–7329.

Van Wagner, C. E., and T. L. Pickett (1985), Equations and FORTRAN program for the Canadian forest fire weather index system, Can. For. Serv.

Viegas, D. X., G. Bovio, A. Ferreira, A. Nosenzo, and B. Sol (1999), Comparative study of various methods of fire danger evaluation in southern Europe, *Int. J. Wildland Fire*, *9*(4), 235–246.

Wang, X. L., M. A. Parisien, M. D. Flannigan, S. A. Parks, K. R. Anderson, J. M. Little, and S. W. Taylor (2014), The potential and realized spread of wildfires across Canada, *Global Change Biol.*, *20*(8), 2518–2530.

Westerling, A. L., H. G. Hidalgo, D. R. Cayan, and T. W. Swetnam (2006), Warming and earlier spring increase western US forest wildfire activity, *Science*, *313*(5789), 940–943.

Wolfe, R. E., D. P. Roy, and E. Vermote (1998), MODIS land data storage, gridding, and compositing methodology: Level 2 grid, *IEEE Trans. Geosci. Remote Sens.*, *36*(4), 1324–1338.

Wooster, M. J., B. Zhukov, and D. Oertel (2003), Fire radiative energy for quantitative study of biomass burning: Derivation from the BIRD experimental satellite and comparison to MODIS fire products, *Remote Sens. Environ.*, *86*(1), 83–107.

Wooster, M. J., G. Roberts, G. L. W. Perry, and Y. J. Kaufman (2005), Retrieval of biomass combustion rates and totals from fire radiative power observations: FRP derivation and calibration relationships between biomass consumption and fire radiative energy release, *J. Geophys. Res.*, *110*, D24311, doi:10.1029/2005JD006318.

Wooster, M. J., G. Roberts, A. M. S. Smith, J. Johnson, P. Freeborn, S. Amici, and A. T. Hudak (2013), Thermal remote sensing of active vegetation fires and biomass burning events, in "Thermal Remote Sensing", edited by C. Kuenzer and S. Dech, chap. 18, Springer, Heidelberg.